universität innsbruck
Fakultät für Mathematik,
Informatik und Physik

Bachelor Thesis

Generative modeling of spin systems

Florian Fürrutter

November 1, 2022

Supervisor: Ass.-Prof. Dr. Mathias S. Scheurer

Institute for Theoretical Physics

Eidesstattliche Erklärung

Ich erkläre hiermit an Eides statt durch meine eigenhändige Unterschrift, dass ich die vorliegende Arbeit selbständig verfasst und keine anderen als die angegebenen Quellen und Hilfsmittel verwendet habe. Alle Stellen, die wörtlich oder inhaltlich den angegebenen Quellen entnommen wurden, sind als solche kenntlich gemacht.

Ich erkläre mich mit der Archivierung der vorliegenden Bachelorarbeit einverstanden.

Abstract

Machine learning has experienced an uninterrupted growth over the last few years. Advancements in research and computation hardware allow the application of neural networks in a diverse spectrum. Motivated by remarkable results in generating indistinguishable fake images of humans and landscapes (e.g., Deep-fakes) physical problems are getting more attention. In this thesis, we look at generative adversarial networks (GAN) which are able to learn the hidden distribution of a training set sampled from a physical system. Based on conditional GANs we show the Ising model can be learned and reproduced at unseen thermodynamic control parameters. We propose the SpinGAN architecture that catches the phase transition of the 2D Ising model with great accuracy. The deterministic neural network allows us to evolve single distinct Ising states through the temperature range. Utilizing the exact differentiation of the network we present a new GAN fidelity to identify critical temperatures without knowledge of the physical system.

Contents

Introduction

In the last decade, neural networks became the most relevant machine learning technique. Advancements in hardware performance allowed larger networks to be trained. Neural networks have an enormous field of application due to their excellent generalization properties [7, 27]. Ongoing research, especially in generative models, showed that it is possible to generate indistinguishable fake images (e.g., Deep-fakes) from training datasets consisting of real-world photos [10].

Remarkable results in image generation motivated the appliance of neural networks for physical systems. In this thesis, we focus on spin systems which are important in many physical fields. For example, in solid state physics spin models are used to model ferromagnetic behaviour. The simplest description is the Ising model. We use the latter, analytically solved in two dimensions, as our benchmark system for the machine learning performance measure. The generative modeling of the Ising model was the object of research in [18] and [14]. The authors showed the generation of Ising model states is possible with good accuracy. Furthermore, in [23] generative modeling is used for phase detection in the XY model.

We expand the ideas of the mentioned papers and apply different generative adversarial networks (GAN) to the 2D Ising model. The generation is done with a conditional GAN which is able to generate states at any given temperature. The training set is based on Monte Carlo simulation at discrete temperature points. Our contribution is the comparison of a state-of-art image generation architecture [10] to a simpler model [22] in a physical setting. Furthermore, we propose the SpinGAN architecture that outperforms the other models. Finally, the critical point detection of [23] is modified and shown to peak at the critical vicinity.

The thesis is structured in the following way. First, we introduce the basics of neural networks and generative modeling. Then the Ising spin model is explained and we look into classical Monte Carlo simulation methods. In the next two chapters, we present three generative adversarial network architectures and implementation details. Especially, we define performance metrics and a new fidelity measure for phase transitions. Followed by the most important chapter in which we present and compare the results of our proposed GAN architecture called SpinGAN. The thesis is concluded with a short discussion and summary.

1. Neural networks

The most famous machine learning technique, neural networks, is a numerical method capable of modeling an enormous spectrum of problems. In 1943 the subject started with the creation of the first computational model of a neural network [16].

Neural networks are an arrangement of many basic units, namely neurons. Initially, the artificial neurons were biological motivated and designed to resemble the behaviour of biological found neurons. A single neuron receives signals either from other neurons or external inputs. Within the cell body, the inputs $\mathbf{x}$ get combined and the neuron outputs a corresponding signal y to the next node in the network. The modern translation into a mathematical model is shown in Figure 1.1. First, the inputs get multiplied individually with corresponding weight training parameters $\mathbf{w}$. These weights are the influence strength of the individual inputs. The weighted inputs are summed up and an additional training parameter called the bias b is added. With this, we are able to model any affine transformation. For real problems this will hardly be sufficient, therefore we apply the so-called activation function f on the summation result. The key point of the activation function is nonlinearity. Recall, that nonlinear systems often behave chaotically. This is a reason why we are able to utilize neural networks as universal approximators [7, 27]. The latter is an important point, in practice, these networks are very powerful approximators but never exact.

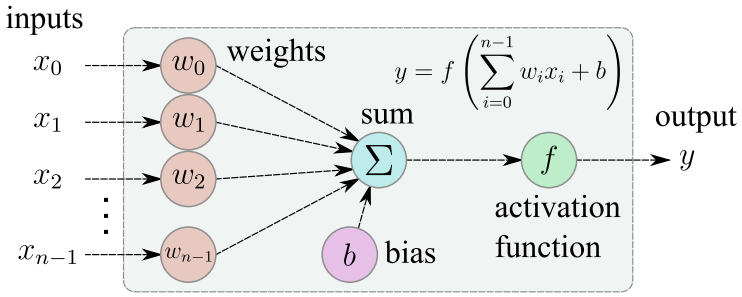

Figure 1.1.: Mathematical model of a single neuron. Given an input vector $\mathbf{x}$ with size n the neuron outputs a scalar y.

Within a network the activation function to choose is arbitrary. At the network output, one has to consider the model's purpose to utilize the correct activation function. The choice is depending on the output variables themselves, e.g., for object classification they will be probabilities and for estimating the temperature of some state the output is continuous and positive. The activation function ideally resembles this behaviour. Common activation functions are presented in Figure 1.2. The rectified linear unit (ReLU) Equation 1.1 is the non-negative identity and an example for the mentioned temperature estimation. LeakyReLu Equation 1.2 consists of two differently sloped lines and is commonly used within a network. When the problem demands a binary classification

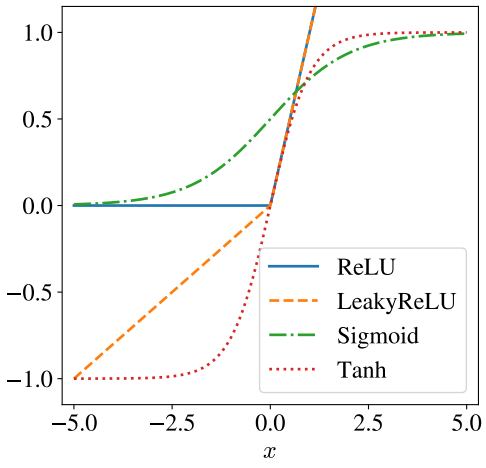

Figure 1.2.: Graphs of activation functions. For LeakyReLU $\alpha = 0.2$ is used.

Common activation functions:

$$f_1(x) = \max(0, x) \quad \dots \text{ ReLU} \tag{1.1}$$

$$f_2(x) = \begin{cases} x: & x \geq 0 \\ \alpha x: & x < 0 \end{cases} \quad \dots \text{ LeakyReLU} \tag{1.2}$$

$$f_3(x) = \frac{1}{1 + \exp(-x)} \quad \dots \text{ Sigmoid} \tag{1.3}$$

$$f_4(x) = \tanh(x) \quad \dots \text{ Tanh} \tag{1.4}$$

then the sigmoid function Equation 1.3 is used at the output. The reason is that logistic regression tells us the probability for binary draws has a sigmoid dependency. In chapter 2 we discuss the Ising model with output variables ± 1. Hence, we use the hyperbolic tangent Equation 1.4 as the output activation function to directly model the output.

1.1. Dense layer

A neural network can contain numerous neurons. Normally, networks are abstracted in terms of layers. Each layer is a collection of neurons arranged in some specific way. Furthermore, a single layer has several defined inputs and outputs. Model architectures specify the type of utilized layers and how to connect them.

The simplest layer is the dense-connected layer where a bunch of neurons are placed in parallel. They share the same inputs $\mathbf{x}$ that are connected to every neuron, with its corresponding weights and bias. Every neuron has one output y. Hence, the dense layer has the same number of outputs $\mathbf{y}$ as the number of neurons in the layer.

Definition 1.1.1 (Dense connected layer)**.** *Consider a layer with n inputs $\mathbf{x} \in \mathbb{R}^n$ and m parallel neurons with outputs $\mathbf{y} \in \mathbb{R}^m$. We call the layer with the operation*

$$\mathbf{y} = f(\mathbf{W}\mathbf{x} + \mathbf{b}) \tag{1.5}$$

a dense connected layer. Here $\mathbf{W} \in Mat_{m,n}(\mathbb{R})$ is the weight matrix, $\mathbf{b} \in \mathbb{R}^m$ the bias vector and f an activation function that is applied element-wise.

An arrangement of layers in series is called a straight feedforward configuration. Like a chain, starting from the model input, every layer is only connected to the next one until the model output is reached. We present an example of such a Deep-Neural-Network in Figure 1.3. A hidden layer is a layer that is not model input or output. The word deep refers to the fact that hidden layers exist in the network.

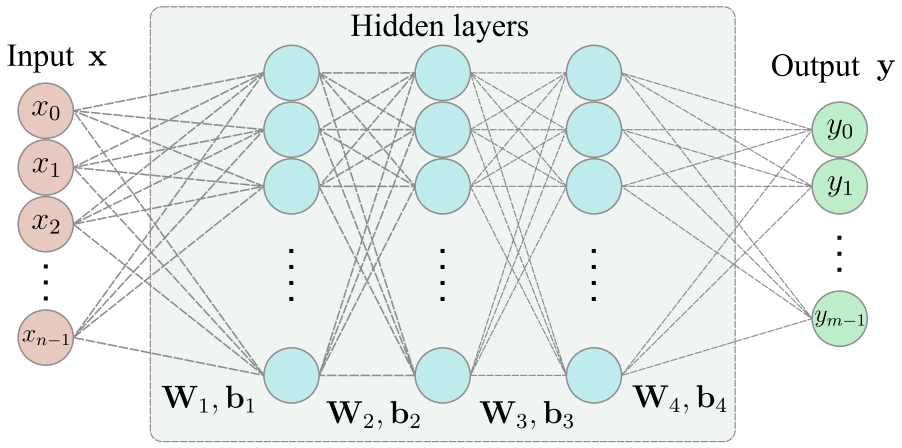

Figure 1.3.: Example of a Deep-Neural-Network (DNN). A straight feedforward configuration of three hidden layers, an input $\mathbf{x}$ and output $\mathbf{y}$. Each connection step has its weights $\mathbf{W}_i$ and biases $\mathbf{b}_i$. The neuron count per layer is an arbitrary number depending on the architecture.

A nice property of these networks is the proven universal function approximation capability, summarized in the *universal approximation theorem* [7, 27]. The general statement is that a dense network with one hidden layer is sufficient to approximate every continuous function with a compact domain to any accuracy. No prediction about the number of neurons in the hidden layer or how to optimize the weights (training parameters) is made. The problem remains that training neural networks is still not trivial.

In practice, networks only consisting of dense layers suffer from additional issues that limit their accuracy. For the following points, it is helpful to imagine images of a chair with the goal to train a network that tells us where the chair is located in the image.

- **Not considering locality:** In the sense that every neuron is connected to all the inputs disregarding their position. Shuffling the model input (e.g., an image) for the whole data set only changes the location of the weights in $\mathbf{W}$ and not their value. Clearly, for us, a shuffled image of a chair will look more like random noise than a chair.
- **Not translation invariant:** A chair remains a chair, regardless of where in the image it is located. The dense network has different weights for different inputs. Thus, a translation in the input also changes the corresponding weights.
- **Overfitting:** A well-known problem of neural networks where the accuracy on the training set is high, but performance on test data is poor. Especially too large/deep dense networks with too many training parameters suffer from this problem.

1.2. Convolution layer

Motivated by visual cortex cells and the translation invariance problem of dense layers the convolutional layer emerged [4, 13]. The key idea is to consider a layer of only a few

neurons called the kernel or filter. The inputs of these neurons are only connected to local layer inputs. Moving the kernel over the whole input (image or tensor) allows for translation invariant local feature extraction. Mathematical we call such an operation convolution. One kernel produces one output (image or tensor). Normally one uses n kernels per convolutional layer to extract multiple features of the same input. The number n has multiple names: filter-size, features or output channels.

Definition 1.2.1 (2D Convolutional layer)**.** *Consider an equilateral kernel size k (for simpler notation $k_x = k_y = k$) and a filter-size of n. The layer input tensor has the height h, width w and c channels. With $i = 1, \dots, n$ the feature index: kernel $\mathbf{K}^{(i)} \in Mat_k(\mathbb{R}^c)$ and $\mathbf{Y}^{(i)} \in Mat_{h',w'}(\mathbb{R})$. Further, the input $\mathbf{X} \in Mat_{h,w}(\mathbb{R}^c)$ and bias $\mathbf{b} \in \mathbb{R}^n$. We call a layer with the operation*

$$\mathbf{Y}^{(i)} = f(\mathbf{K}^{(i)} * \mathbf{X} + b_i \cdot \mathbb{1}_{h',w'}) \tag{1.6}$$

a convolutional layer with the concatenation of all $\mathbf{Y}^{(i)}$ as the layer output. Here $\mathbb{1}$ is the matrix of ones, f an activation function and $*$ is the discrete convolution operation

$$\left(\mathbf{K}^{(i)} * \mathbf{X}\right)_{j,l} = \sum_{\alpha,\beta=0}^{k-1} \mathbf{k}^{(i)}_{\alpha,\beta} \cdot \mathbf{x}_{j+\alpha-d,\, l+\beta-d} \quad \textit{with} \quad d = \begin{cases} (k-1)/2 & : k \textit{ odd} \\ k/2 - 1 & : k \textit{ even} \end{cases}. \tag{1.7}$$

Note, elements of $\mathbf{K}^{(i)}, \mathbf{X}$ are vectors $\mathbf{x}, \mathbf{k} \in \mathbb{R}^c$. The range of j, l and the output dimensions h', w' depend on the stride s and padding p (e.g., zeros, periodic, nearest, ...).

The stride s indicates how many pixels the kernel is moved for every evaluation of Equation 1.7 (effectively downscaling by a factor s) and the input $\mathbf{X}$ is padded with p pixels. We can calculate the output dimensions of such a 2D convolutional layer with

$$(h', w', c') = \left(\left\lfloor \frac{h - k + 2p}{s} + 1 \right\rfloor, \left\lfloor \frac{w - k + 2p}{s} + 1 \right\rfloor, n \right), \tag{1.8}$$

where $\lfloor \cdot \rfloor$ is the floor operator. Furthermore, the convolution operator can be written as a matrix vector multiplication. For this, we have to construct a sparse matrix $\mathbf{G}$ with circular double blocked matrices and flatten out the matrix $\mathbf{X}$ into a vector. The construction is not hard but tedious. Hence, we do not write it explicitly here. Just note that matrix multiplication can be easily optimized and parallelized.

For one convolutional layer, we have the training parameters of the kernel $\mathbf{K} \in \mathbb{R}^{n \times k_x \times k_y \times c}$ and the bias $\mathbf{b} \in \mathbb{R}^n$. The parameters stay the same when we change the input dimensions height h and width w. Usually one combines convolutional and dense layers in a straight feedforward model architecture for classification tasks.

1.3. Training

We train feedforward neural networks with the backpropagation algorithm, first applied to neural nets in 1974 [25]. Backpropagation is used for efficiently minimizing the expectancy value of a loss/cost/energy function $\mathcal{L}$. One is likely familiar with the mean

squared error from linear regression. This is an example of extremizing a defined loss function. In our case, the networks have numerous training parameters. Therefore, the optimization landscape of $\mathcal{L}$ possesses a high complexity with many local minima. The optimization is based on the gradient of the loss function with respect to the training parameters. Backpropagation describes the method of calculating the gradients of every layer consecutively from the back. Hence, derivatives given by the chain rule are evaluated only once and the algorithm removes this redundancy from direct gradient calculation.

In this section, we regard the neural network as a black-box $\text{Net}(\mathbf{x})$ with some input $\mathbf{x}$. The model weights $\mathbf{W}$ are all training parameters (weights and biases combined). The goal is to iteratively minimize the loss function (e.g., mean squared error) evaluated utilizing the training data while varying the model weights

$$\mathcal{L} = \mathcal{L}\left(\text{Net}(\mathbf{x}), \mathbf{y}\right) \quad \text{with} \quad \{\mathbf{x}, \mathbf{y}\} \text{ the training set.} \tag{1.9}$$

The training set consists of inputs $\mathbf{x}$ and corresponding outputs $\mathbf{y}$ (labels). We consider the gradient of $\mathcal{L}$ in the weight space and evaluate $\nabla_{\mathbf{W}}\mathcal{L}$ while considering the training set as constant. How to update the weights according to the gradient is specified by the used optimizer algorithm. A simple example is the stochastic gradient descend optimizer.

Definition 1.3.1 (Stochastic gradient descend, SGD)**.** *One iterative update of the model weights* $\mathbf{W}$ *is done with*

$$\mathbf{W}' = \mathbf{W} - \lambda \frac{1}{n} \sum_{i=1}^{n} \nabla_{\mathbf{W}} \mathcal{L}(\text{Net}(\mathbf{x}_i), \mathbf{y}_i) \quad \textit{where} \quad (\mathbf{x}_i, \mathbf{y}_i) \in \text{Train subset.} \tag{1.10}$$

Here n is called the batch or mini-batch size and λ is the learning rate hyperparameter. Further, the train subset is drawn consecutively from the whole train set.

The word stochastic refers to the average over the drawn subsets. A whole pass of the train set is called an epoch. Choosing the batch size n is a trade-off between how many weight updates are done per epoch and better global minima convergence. Furthermore, fewer updates per epoch are more efficient because writing weights is expensive. In Figure 1.4 we illustrate the iterative updating process with convergence into a local minimum.

The SGD can be improved to insure faster convergence and local minima escape capabilities. There exist many such optimizer algorithms, each with their pro and cons. An often used choice is the Adam (Adaptive Moment Estimation) optimizer [12].

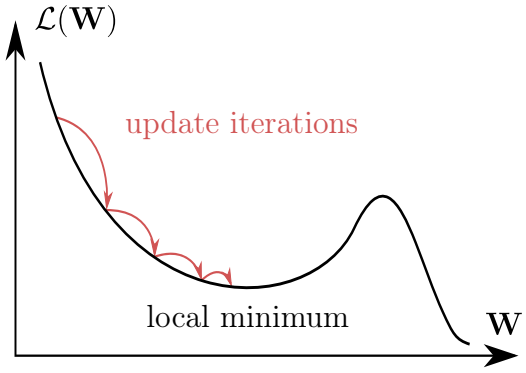

Figure 1.4.: Illustration of the SGD optimizer with iterative updates.

1.4. Generative adversarial networks

The concept of a generative adversarial network (GAN) [5] is a special type of neural network architecture. GANs are generative unsupervised learning approaches where we do not supply a training set of input-output tuples $(\mathbf{x}, \mathbf{y})$. Instead, we sample data from an unknown distribution (e.g., taking landscape photos) and note it as real data. The GAN then learns to generate samples from the hidden distribution. Hence, the GAN learns the distribution implicitly. The method is capable to generate unseen photo-realistic images of provided real data [10]. This inspires us to apply GAN techniques to physical systems.

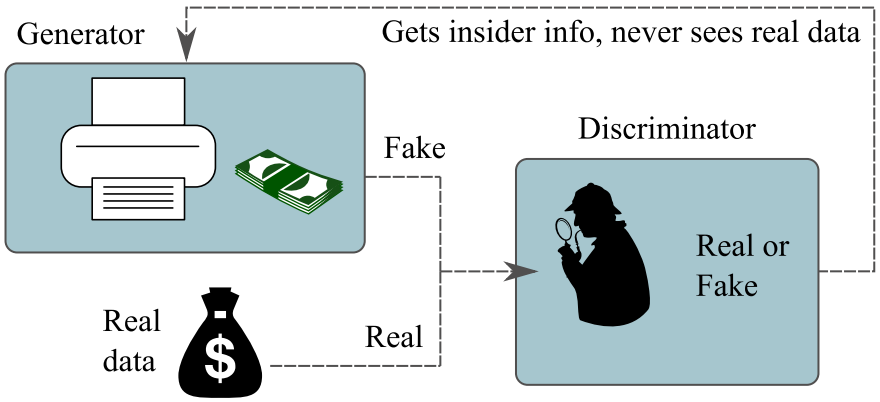

Figure 1.5.: Conceptual illustration of a generative adversarial network (GAN), which goal is to produce fake data that is indistinguishable from the training set. The generator learns to produce these fake samples and gets feedback from the discriminator. The training data is only provided to the discriminator, which has to classify samples as real or fake. These players must stay in equilibrium for convergence.

The GAN architecture specifies two connected networks called generator and discriminator. The generator is the part that generates fake images and the discriminator's goal is to judge if a provided sample is real or fake. In Figure 1.5 a conceptual illustration of the GAN working principle is shown.

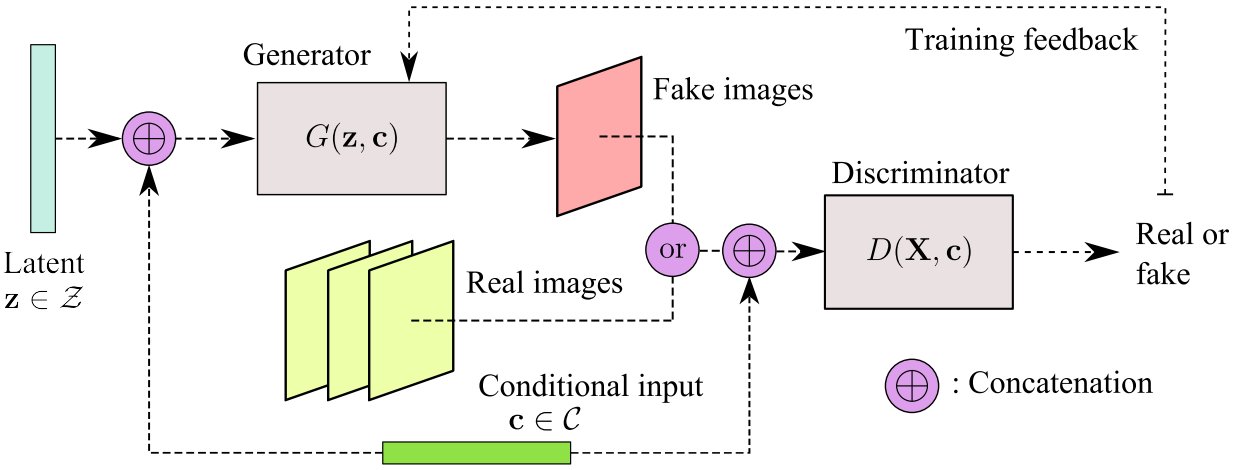

Figure 1.6.: Conditional GAN. The generator gets the concatenation of a latent vector $\mathbf{z}$ and a conditional vector $\mathbf{c}$ as input. The condition $\mathbf{c}$ with a data sample $\mathbf{X}$ is presented to the discriminator. This tuple is either generated or from the training set.

1.4.1. Mathematical description

We are interested in the conditional generative adversarial network, a variant of GAN. Here, we extend the GAN with an additional input that allows us to specify what data we want to generate. The conditional input $\mathbf{c}$ can consist of any known property of the real data. In our case, the condition will be the temperature of the physical system.

A block diagram of the conditional GAN is presented in Figure 1.6. The generator $G : (\mathbf{z}, \mathbf{c}) \mapsto \mathbf{X}$ takes as input a latent vector $\mathbf{z}$ sampled from the latent space $\mathcal{Z}$. Additionally, in the case of a conditional GAN also a condition $\mathbf{c}$ from condition space $\mathcal{C}$. The discriminator $D : (\mathbf{X}, \mathbf{c}) \mapsto (0, 1)$ receives a real or fake sample $\mathbf{X}$ and optionally the corresponding specifier $\mathbf{c}$. Furthermore, we extend the architecture with an auxiliary network $A : \mathbf{X} \mapsto \mathbf{c}$ that trains on real data to classify the condition $\mathbf{c}$. The pre-trained auxiliary network then classifies fake samples and provides more information to the generator. It was shown this is helping to stabilize the GAN training [19, 23]. Mathematical we write the specific GAN optimization goal of this thesis as:

Definition 1.4.1 (Conditional GAN, player goals)**.**

Generator:

$$\min_G \Big(\quad \mathbb{E}_{\mathbf{z}\sim p_z,\, \mathbf{c}\sim p_c} \left[\mathcal{L}_G(D(G(\mathbf{z}, \mathbf{c}), \mathbf{c}), \text{Real})\right] \tag{1.11}$$

$$+ \mu \quad \mathbb{E}_{\mathbf{z}\sim p_z,\, \mathbf{c}\sim p_c} \left[\mathcal{L}_A(A(G(\mathbf{z}, \mathbf{c})), \mathbf{c})\right] \Big) \tag{1.12}$$

Discriminator:

$$\min_D \Big(\quad \mathbb{E}_{\mathbf{z}\sim p_z,\, \mathbf{c}\sim p_c} \left[\mathcal{L}_D(D(G(\mathbf{z}, \mathbf{c}), \mathbf{c}), \text{Fake})\right] \tag{1.13}$$

$$+ \quad \mathbb{E}_{(\mathbf{X},\mathbf{c})\sim p_{\text{data}}} \left[\mathcal{L}_D(D(\mathbf{X}, \mathbf{c}), \text{Real})\right] \tag{1.14}$$

$$+\frac{\gamma}{2} \quad \mathbb{E}_{(\mathbf{X},\mathbf{c})\sim p_{\text{data}}} \left[\left\|\boldsymbol{\nabla}_{(\mathbf{X},\mathbf{c})} D(\mathbf{X}, \mathbf{c})\right\|^2\right] \Big) \tag{1.15}$$

Auxiliary network:

$$\min_A \Big(\; \mathbb{E}_{(\mathbf{X},\mathbf{c})\sim p_{\text{data}}} \left[\mathcal{L}_A(A(\mathbf{X}), \mathbf{c})\right] \Big) \tag{1.16}$$

Here μ,$\gamma \in \mathbb{R}^+$ are hyperparameters. The expressions should be minimized by varying the model parameters of G, D and A. Each player has a corresponding loss function $\mathcal{L}$. Note that the generator and discriminator have contradictory goals and need to be in equilibrium. Equation 1.15 is a regularizer term. It penalizes large discriminator gradients evaluated for real data. With this GAN convergence was shown [17] when model parameters are initialized sufficiently close to the equilibrium point.

1.4.2. Convergence

Generative adversarial networks are still objects of ongoing research. Hence, there exist a few not completely solved common problems. We want to give the reader a short overview of the most common problems without too much detail.

Vanishing gradient: In flat areas of the loss function landscape small gradients $\nabla\mathcal{L}$ occur. Small derivatives get multiplied together, because of the chain rule. Thus, the final result gets tiny. The weight optimizer use the gradient to update the model parameters. If the gradient value vanishes we get stuck. The weights will not change noticeably. We call this the vanishing gradient problem. Some authors suggest this happens when the discriminator is too good [1]. Attempts in choosing specific loss functions (e.g., Wasserstein [2]) can yield improvements.

Equilibrium states: Generally, the GAN architecture defines an optimization game between different players (see Definition 1.4.1). These players train on one another and try to optimize their contradicting goals. Ideally, no player dominates and the GAN as a whole converges to an equilibrium state. GAN equilibrium states are fleeting rather than stable fix-points. If the generator is good enough to generate perfect fake images then the discriminator can only guess if a presented state is real or fake. This random feedback will destroy the equilibrium state of the generator and the overall model performance collapses.

Mode collapse: Choosing the wrong GAN architectures or parameters often leads to the problem of mode collapse. Here, the generator G maps the latent space $\mathcal{Z}$ only to a subset of the desired image space. Sometimes even to a single image, completely ignoring the latent vector. Intuitively the reason is clear, the generator found similar images that fool the discriminator. Hence, using only these images greatly reduces the generator minimization expression.

Note, in practice the mentioned convergence issues are dealt with by utilizing some heuristic practical tricks. GAN training is very sensitive to changes in hyperparameters. In combination with the unstable equilibrium state, the tuning of the training parameter can be quite hard in general.

2. Ising model

Advancements in *quantum theory*, especially the inference of the spin concept, made a basic understanding of para- and ferromagnetism in solid matter possible. In 1924 a statistical physics model of ferromagnetism was proposed by Ernst Ising [8], namely the broadly known Ising model. The mathematical model describes spins at discrete lattice sides that can be considered either classically or quantum theoretically. We restrict ourselves here to the classical Ising model where the spin at lattice point i is discrete.

Definition 2.0.1 (Classical Ising model)**.** *The general Hamiltonian is given by:*

$$H = -\sum_{\langle i,j \rangle} J_{i,j}\ \sigma_i \sigma_j - \sum_i h_i \sigma_i. \tag{2.1}$$

Here $\langle i,j \rangle$ means the sum over all adjacent lattice sides and $J_{i,j}$ is the exchange interaction strength between spin i and j. The influence of an external field is denoted as h_i. The discrete spins are either up or down $\sigma_i \in \{\pm 1\}$.

This Hamiltonian can be studied for any dimensional lattices where the number of nearest neighbours z is the only thing that changes, e.g., for two dimensions a spin has four neighbouring spins $z = 4$ and in three dimensions $z = 6$.

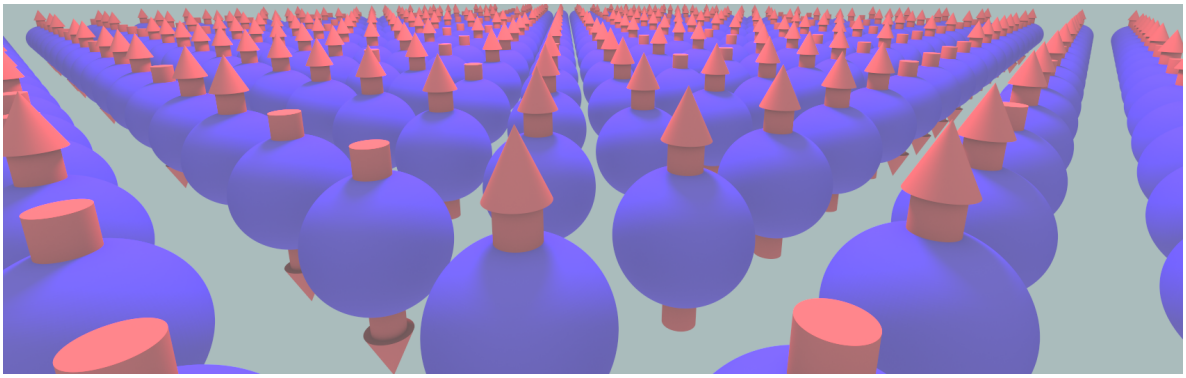

Figure 2.1.: Illustration of a two-dimensional lattice with spins either pointing up or down.

In this thesis we focus on the two-dimensional case with a global interaction strength $J = J_{i,j} > 0$ and no external field $h_i = 0$. Therefore, Equation 2.1 reduces to

$$H = -J \sum_{\langle i,j \rangle} \sigma_i \sigma_j. \tag{2.2}$$

This was the first model to exhibit a continuous phase transition for positive temperatures $T > 0$. Statistical physics yields with the canonical ensemble a critical temperature T_c, which divides the temperature range into two phases. For $T < T_c$ the spins will be mostly aligned and the system ferromagnetic. On the other hand, for $T_c < T$ the thermodynamic fluctuations randomly flip the spins and the system behaves paramagnetic with no mean magnetization. In 1944 an analytic solution of the critical temperature was derived by Lars Onsager [20]

$$T_c = J\frac{2}{k_\mathrm{B}\ln\left(1+\sqrt{2}\right)} \approx 2.269\frac{J}{k_\mathrm{B}}, \tag{2.3}$$

where k_B is the Boltzmann constant. For further discussion, the lattice is squared and finite with L spins per side and $N = L^2$ total spins. We consider periodic boundary conditions for our finite system sizes. We note a configuration or microstate of the system with $\mathbf{\Sigma} = (\sigma_0, \sigma_1, \ldots, \sigma_{N-1}) \in \{\pm 1\}^N$.

2.1. Important observables

Statistical physics and thermodynamics specify many observables. Here, the most important one is the magnetization m which is the order parameter for this Ising system. The energies E are the eigenvalues of the Hamiltonian and specify the macrostates. Further, the magnetic susceptibility χ and the correlation length ξ characterize the critical temperate T_c at which their values diverge in the thermodynamic limit.

2.1.1. Magnetization

The magnetization m is the order parameter of the Ising model and given with the normalized sum over the spins

$$m := \frac{1}{N}\sum_{i=0}^{N-1}\sigma_i. \tag{2.4}$$

Naively looking at the $\mathbb{Z}_2$ symmetry of the Hamiltonian may tempt one to think m is always vanishing on average. The argument is that every microstate has a mirrored state with the same energy and therefore the same probability. This is only the case for temperatures above the critical temperature. Below T_c spontaneous symmetry breaking occurs and $\langle m\rangle \neq 0$. An observable with this behaviour is called order parameter.

Corollary 2.1.1. *The mean of one spin equals the mean of the total magnetization*

$$\langle\sigma_i\rangle = \frac{1}{N}\sum_{i=0}^{N-1}\langle\sigma_i\rangle = \left\langle\frac{1}{N}\sum_{i=0}^{N-1}\sigma_i\right\rangle = \langle m\rangle\,. \tag{2.5}$$

Proof. One uses the translation invariance of the Ising model to apply the spatial average and then the linearity of the mean. □

2.1.2. Energy

The energy E classifies a macrostate. It includes all microstates $\mathbf{\Sigma}$ with the same energy. We get the energy by simply inserting the microstate into the Hamiltonian

$$E := \frac{1}{N} H(\mathbf{\Sigma}) = -\frac{J}{N} \sum_{\langle i,j \rangle} \sigma_i \sigma_j. \tag{2.6}$$

To compare the energy for different system sizes we normalize the energy per spin.

2.1.3. Magnetic susceptibility

The magnetic susceptibility χ is the linear response coefficient of the system to an applied magnetic field h

$$\chi := \left(\frac{\partial m}{\partial h} \right)_{T,\, h=0}. \tag{2.7}$$

For the direct usage of this definition, we have to consider the general Hamiltonian from Equation 2.1 and simulate the system for different external field strengths. Statistical physics allows us to rewrite χ such that the simpler Equation 2.2 is sufficient.

Theorem 2.1.1. *The magnetic susceptibility can be evaluated with fluctuations of the magnetization in thermodynamic equilibrium*

$$\chi = \left(\frac{\partial m}{\partial h} \right)_{T,\, h=0} = \frac{N}{k_B T} \operatorname{Var}\left[|m|\right] = \frac{N}{k_B T} \left(\left\langle m^2 \right\rangle - \left\langle |m| \right\rangle^2 \right). \tag{2.8}$$

Proof. Appendix B □

2.1.4. Spin-spin correlation

The spin-spin correlation is defined as the covariance between two spin variables

$$G_c(i,j) := \operatorname{Cov}\left[\sigma_i, \sigma_j\right] = \left\langle \sigma_i \sigma_j \right\rangle - \left\langle \sigma_i \right\rangle \left\langle \sigma_j \right\rangle. \tag{2.9}$$

Recall the spin σ_i is located at the lattice point $\mathbf{r}_i$. Our Ising Hamiltonian Equation 2.2 is translation invariant. Hence, the correlation function only depends on the relative vector $\mathbf{r} = \mathbf{r}_j - \mathbf{r}_i$ between the spin positions

$$G_c(\mathbf{r}) = G_c(\mathbf{r}_i, \mathbf{r}_i + \mathbf{r}). \tag{2.10}$$

Because G_c is independent of $\mathbf{r}_i$ we average over all combinations where $\mathbf{r}$ occurs and therefore improve our estimation. With Corollary 2.1.1 we get

$$G_c(\mathbf{r}) = \frac{1}{N} \sum_{i,j=0}^{N-1} \delta_{(\mathbf{r}_i - \mathbf{r}_j), \mathbf{r}} \left[\left\langle \sigma_i \sigma_j \right\rangle - \left\langle m \right\rangle^2 \right]. \tag{2.11}$$

Theorem 2.1.2. *The spin-spin correlation function can be calculated efficiently with a fast Fourier transform:*

$$G_c(\mathbf{r}) = (\mathcal{F}^{-1} g_c)(\mathbf{r}) \quad \text{with} \quad g_c(\mathbf{k}) = \frac{1}{N} \begin{cases} \left\langle |(\mathcal{F}\sigma_i)(\mathbf{k})|^2 \right\rangle : & \mathbf{k} \neq 0 \\ 0 : & \mathbf{k} = 0 \end{cases}. \tag{2.12}$$

Proof. Appendix B □

The Hamiltonian is also rotation invariant in discrete directions. Further, the correlation function only depends on the absolute value of the distance vector $\mathbf{r}$ for large distances

$$G_c(r) \underset{r\to\infty}{\cong} G_c(\mathbf{r}) \quad \text{with} \quad r = |\mathbf{r}|. \tag{2.13}$$

We improve the estimator by averaging over all angular directions in a distance of r. Note that $r \leq N/2$. This is because we utilize periodic boundary conditions and the correlation function is therefore also periodic in r. Analytic results from *mean field theory* state for $T \neq T_c$

$$G_c(r) \propto \exp\left(-\frac{r}{\xi}\right), \tag{2.14}$$

where ξ is defined as the correlation length. We estimate ξ by fitting Equation 2.14 to the angular averaged result of Equation 2.13.

2.2. Phase transition

The Ising model without external field undergoes a phase transition at T_c for a dimension $d \geq 2$. The transition is classified by the continuous order-parameter m.

At high temperatures $T_c < T$ the mean magnetization vanishes to thermodynamic fluctuations $\langle m \rangle = 0$ and the external field response is paramagnetic. Low temperatures allow spontaneous symmetry breaking to occur and align most of the spins. A mean magnetization $\langle m \rangle \neq 0$ lets the system behave ferromagnetic.

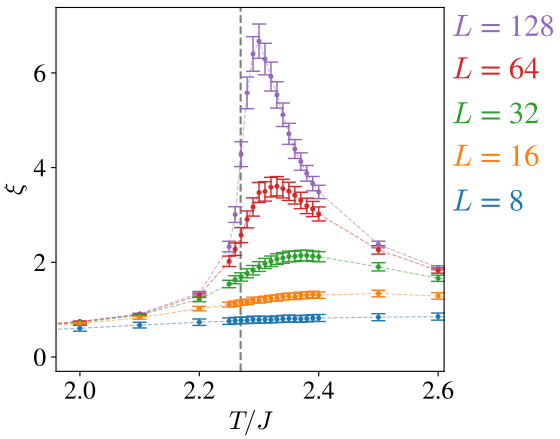

Figure 2.2.: Correlation length ξ for different system sizes L. The critical temperature T_c is marked with a vertical line. Samples generated with Wolff algorithm.

In Figure 2.2 we see peaks in the correlation length approaching T_c from the right for increasingly large finite systems. At the critical temperate the susceptibilities and the correlation length diverge in the thermodynamic limit of an infinite system. In fact, at T_c they follow power laws. This can be shown in *mean field theory* and is further analyzed in the concept of *universality classes*. In our case, this is not relevant. We utilize the 2D Ising model as a benchmark system with analytically known critical temperate given in Equation 2.3.

3. Monte Carlo simulation

Many broadly used computational-physics simulations are based on Monte Carlo (MC) concepts [11, 21, 24]. In numerical Monte Carlo algorithms, the sampling is done randomly. The probabilistic approach allows solving a large set of problems, from optimization to generating samples from any probability distribution.

Machine learning approaches in general and especially generative adversarial networks are techniques that rely heavily on training data. We have to present data to the GAN from which it learns the underlying distribution. In this thesis, we use Monte Carlo techniques to generate states of the Ising model following the probability distribution from the canonical ensemble. These Monte Carlo states are used as the mentioned training set.

The direct sampling of the state distribution is not possible. Hence, we construct a Markov-chain with all possible states of our physical model. The chain is a sequence where we create a configuration and move to the next one until we reach the desired equilibrium. For stable convergence the *condition of detailed balance* [24] must be fulfilled for all state pairs A and B:

$$p_A \cdot w(A \to B) = p_B \cdot w(B \to A). \tag{3.1}$$

Here p_A is the probability to find the system in state A and with $w(A \to B)$ we mean the transition rate from state A to B. Two solutions to Equation 3.1 are given with the Metropolis–Hastings and Wolff algorithms. The generation of the state-sample-set is done, regardless of the update algorithm, with the following steps:

1. Initialize a random/arbitrary state $\mathbf{\Sigma}$.
2. Do Update$(\mathbf{\Sigma}, T, J)$ until the thermodynamic equilibrium is reached.
3. In order to reduce autocorrelation, do n-times Update$(\mathbf{\Sigma}, T, J)$.
4. Store $\mathbf{\Sigma}$ and/or calculate observables of the current state.
5. Repeat from step 3 until the number of desired sampled states is reached.

Here the Update$(\mathbf{\Sigma}, T, J)$ function moves along the Markov-chain of the Ising model and creates new states $\mathbf{\Sigma} \to \mathbf{\Sigma}'$ from existing ones. The control parameter T and model constant J are additional inputs. The definition of Update$(\mathbf{\Sigma}, T, J)$ is varying by the used algorithm and declared in the next sections.

3.1. Metropolis–Hastings algorithm

The Metropolis–Hastings algorithm [6] is based on local MC updates. By local, we mean that updates only take into account the state of the nearest neighbouring spins. Considering the system in the canonical ensemble yields for each state $\mathbf{\Sigma}$ the probability

$$p(\mathbf{\Sigma}) = \frac{1}{Z} \exp(-\beta H(\mathbf{\Sigma})), \tag{3.2}$$

where Z is the partition function, H the Hamiltonian and $\beta = 1/k_\mathrm{B}T$. The key idea of Metropolis–Hastings is to consider a random (uniformly sampled) single spin flip $\sigma_i \to (-\sigma_i) \quad (\mathbf{\Sigma} \to \mathbf{\Sigma}')$. Using Equation 3.2 we get the proposal flip probability of the spin at lattice point i with nearest neighbours $\mathrm{NN}(i)$

$$p^{(i)}_\mathrm{proposal} = \frac{p(\mathbf{\Sigma}'(i))}{p(\mathbf{\Sigma})} = \exp(-\beta \Delta E(i)) = \exp\left(-2\beta J \sigma_i \sum_{j \in \mathrm{NN}(i)} \sigma_j\right). \tag{3.3}$$

Hence, the flip probability only depends on the energy difference $\Delta E(i)$ between the configurations before and after the spin i flipped. Is $\Delta E(i)$ negative we always flip, else we sample according to $p^{(i)}_\mathrm{proposal}$. Mathematically the probability is written as $p^{(i)}_\mathrm{flip}$

$$p^{(i)}_\mathrm{flip} = \min\left[1,\ p^{(i)}_\mathrm{proposal}\right]. \tag{3.4}$$

Consider N single flip attempts, following p_flip, a Metropolis–Hastings update step. The UpdateMetropolis$(\mathbf{\Sigma}, T, J)$ function is defined in Algorithm C.1.

3.2. Wolff algorithm

The Wolff algorithm [26] is in the set of cluster-based update methods. Local MC algorithm suffer from critical slow down when sampling near to the critical temperature T_c [11]. This results from the connection between the autocorrelation time $\tau_\mathrm{auto} \sim \xi^z$ $(z > 1)$ and the diverging correlation length ξ (see subsection 2.1.4). The effect can be reduced with cluster updates that change larger portions of the configuration with a single update. With this, the phase space is sampled more even. Thus, fewer updates between measuring configurations are needed. The algorithm efficiency improves a lot near T_c compared to local MC updates.

The key idea of Wolff is to consider two isolated parallel spins next to one another. Flipping both changes nothing. If only one spin flips the energy cost yields a flip probability of $p = \exp(-2\beta|J|)$. We flip entire clusters, with spins of the same orientation, for only the energy cost of the unaligned cluster edges. Hence, we enlarge a cluster to neighbouring parallel spins with the inverse probability

$$p_\mathrm{append} = 1 - \exp(-2\beta|J|). \tag{3.5}$$

The UpdateWolff$(\mathbf{\Sigma}, T, J)$ function, Algorithm C.2, begins with a random initial spin, extends the cluster according to Equation 3.5 and flips the whole cluster.

3.3. Training set

The training set is the distribution sample the generative adversarial network learns to reproduce. We generate configurations of the Ising model from chapter 2 using the Wolff algorithm. For all simulations, we choose the exchange interaction constant $J = 1$. The system size L can be considered arbitrary. For the thermodynamic control parameter T, we sample at 15 distinct temperatures

$$T \in \{1.0, 1.5, 1.8, 2.0, 2.1, 2.2, 2.25, 2.3, 2.35, 2.4, 2.5, 2.6, 2.8, 3.0, 3.4\} . \tag{3.6}$$

The range includes temperatures at all phases of the Ising model. Around the critical temperature $T_c \approx 2.269$ (see Equation 2.3) the density is chosen higher. The simulation steps are listed in chapter 3 and the Wolff updates are explained in section 3.2. We have three simulation parameters

$$n_{\text{thermal}}(T) = 10^3 \cdot T \qquad \ldots \text{chapter 3 list step 2 ,} \tag{3.7}$$
$$n_{\text{sweeps}}(T) = 10^2 \cdot T^2 \qquad \ldots \text{chapter 3 list step 3 ,} \tag{3.8}$$
$$n_{\text{samples}} = 3 \cdot 10^4 \qquad \ldots \text{chapter 3 list step 5 .} \tag{3.9}$$

Here n_{thermal} are the updates until we consider the system in equilibrium. An estimation of this number is possible, one plots the energy in dependence of the updates and looks for convergence. The number n_{sweeps} specifies how many updates we do between measurements of the current state. The latter can be estimated with a binning analysis. The dependence of n_{thermal} and n_{sweeps} on T is because of the Wolff algorithm. The clusters get smaller with larger temperatures, clearly visible in Equation 3.5. To account for that we scale the two simulation parameters with T. We simulate n_{samples} per temperature. In Figure 3.1 a random sample of training states (system size $L = 64$) is presented. One can get a feeling of how the Ising model configurations look at different temperatures.

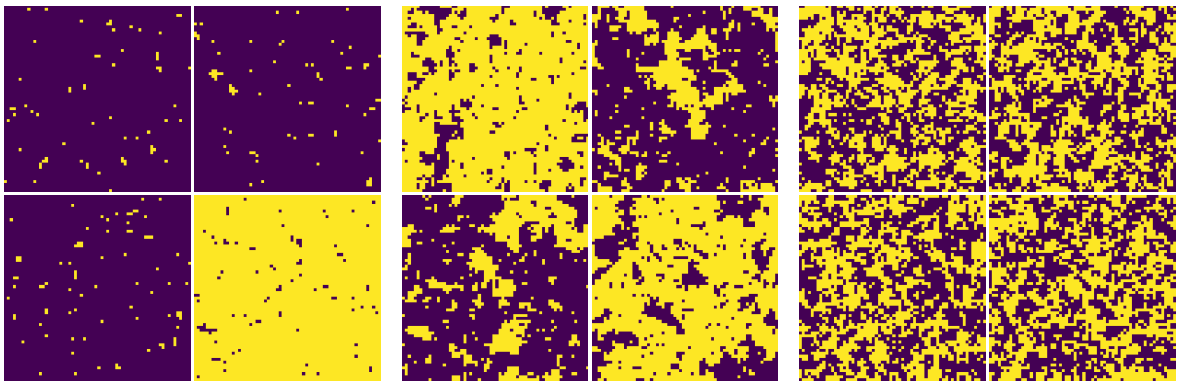

(a) $T = 1.8$ **(b)** $T = 2.3$ **(c)** $T = 3.4$

Figure 3.1.: Presented are randomly sampled states from the training set. The states are generated using the Wolff algorithm. Starting from the left, one sees the ferromagnetic, transition and paramagnetic phases. Utilized is a system size $L = 64$ and an interaction constant $J = 1$.

4. GAN architectures

The goal of our GAN architectures is to learn the implicit distribution from provided states. Our conditional generator takes, additional to the latent vector $\mathbf{z}$, the condition $\mathbf{c}_G = (T, T, T, T)$ as an input. We duplicate the same temperature four times to increase the sensitivity of the generator. For the condition input of the discriminator, we use $\mathbf{c}_D = T$. As the generator loss function $\mathcal{L}_G$, we utilize Wasserstein (Earth-mover) distance [2]. For the discriminator loss $\mathcal{L}_D$, we use cross entropy and for the auxiliary network $\mathcal{L}_A$, the mean squared error. During training, a discriminator gradient penalty (Equation 1.15) $\gamma = 10$ is utilized. As explained in subsection 1.4.1 a pre-trained auxiliary network classifies the condition $\mathbf{c}_D$ from generated samples with $\mu = 5$ (Equation 1.12). All the architectures of this thesis utilize a latent space $\mathcal{Z} \cong \mathbb{R}^a$ with $a = 4096$.

4.1. Spin modeling specific

All considered architectures DC-GAN, StyleGAN2 and SpinGAN have some common properties we discuss in this section. In order to improve the performance of our GAN, we utilize two spin model (Ising model) specific architecture design choices.

- **Periodic bounding:** Our lattice has periodic boundary conditions. In order to make the first convolutional layer of the discriminator consider this, we periodically pad the discriminator input before applying the first layer. With this, the generator gets the corresponding feedback.

- **Amplitude scaling:** Ising states consist of $\sigma_i \in \{\pm 1\}$. Therefore, the activation function of the generator output is chosen as $f = \tanh : \mathbb{R} \mapsto (-1, 1)$. Numerical calculations are the most stable/accurate between 0 and 1. To make the generator more robust we scale the training data to $\sigma_i \in \{\pm 0.7\}$ which corresponds to maximal neuron outputs of $f^{-1}(0.7) \approx 0.87$. For physical evaluation of generator data, the output spins are binarized to ± 1 with the threshold at 0.

4.2. DCGAN

A common choice for the architecture type is the deep convolution GAN (DCGAN) [22]. The model consists of a simple arrangement of convolutional layers and one dense layer. It has good convergence and often performs well for most training parameters. Our results showed that a DCGAN base with additional injection layers (SpinGAN) performed best for our temperature condition. For $L = 64$, the discriminator is presented

in Figure 4.1 and the generator (without the injection layers) in Figure 4.2. Training parameters are the same as SpinGAN from section 4.4.

4.3. StyleGAN2

The StyleGAN2 architecture [10] is designed to generate photo-realistic high-resolution images. These images are shown to be sufficiently good to fool humans (e.g., Deep-fakes). For example, fake images generated from a training set consisting of celebrity photos are almost indistinguishable from real images. Even though the persons on the images do not exist. This is an example of learning implicitly a hidden unknown distribution. The architecture is specified in [9, 10] and we use the tricks from section 4.1. For GAN training we use the Adam optimizer [12] with the same parameters for the generator and discriminator: $(\beta_1 = 0, \beta_2 = 0.9)$. The learning rate has an exponential decay with an initial value of $\lambda = 2 \times 10^{-4}$ and a decay rate of 0.9 per 20 epochs.

4.4. SpinGAN

We propose the SpinGAN architecture. It is based on DCGAN and introduces conditional injection layers. The latter dramatically increases the response of the generated states in dependence on the thermodynamic control parameter T. The discriminator is presented in Figure 4.1. The condition $\mathbf{c}$ is concatenated as extra channels to the input image $\mathbf{X}$. Then the periodic padding is applied (section 4.1). The output activation

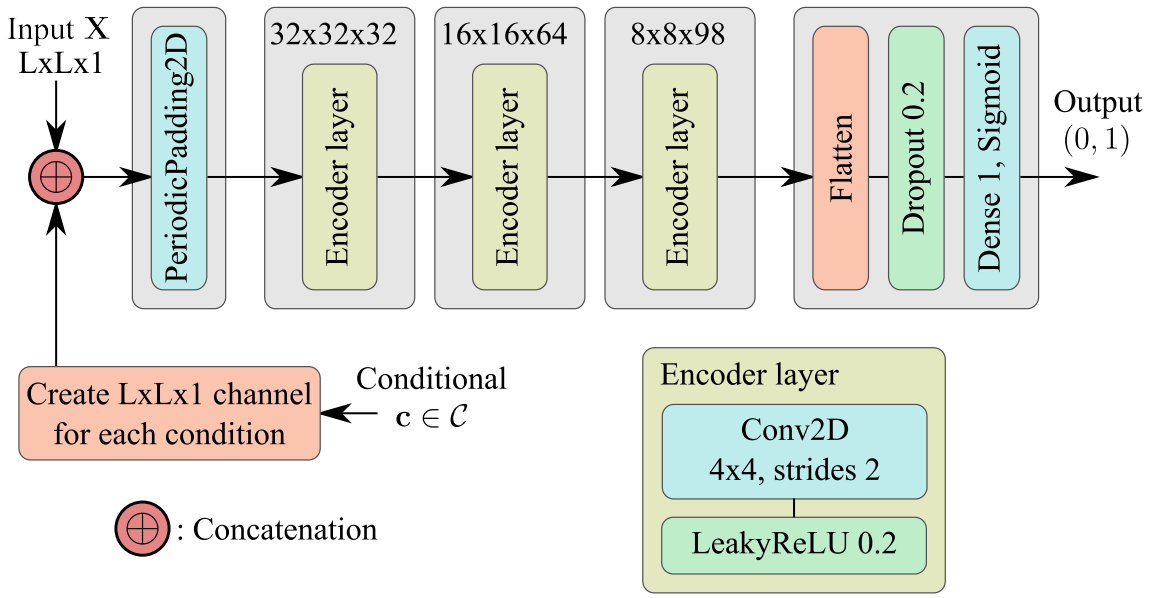

Figure 4.1.: SpinGAN/DCGAN discriminator. Numbers in the top of the gray boxes correspond to the resolution and filter/channel size of the layer. The parameters are given for the system size $L = 64$. Inputs are the images $\mathbf{X}$ (real or fake) and condition $\mathbf{c} = T$ with $T \in \mathbb{R}^+$.

function is a sigmoid because of the binary real or fake classification. During training, the dropout layer sets randomly a percentage of neurons to zero. In our case 20 %. Dropout layers help the GAN to escape local minima and improve the stability of the generator. Furthermore, they simulate noise in real-world data.

We present in Figure 4.2 SpinGAN's generator with the mentioned injection layers. These layers 'remind' the generator at different network depths of the conditional input. In our results, we showed that this improves the sensitivity in the critical range of the phase transition.

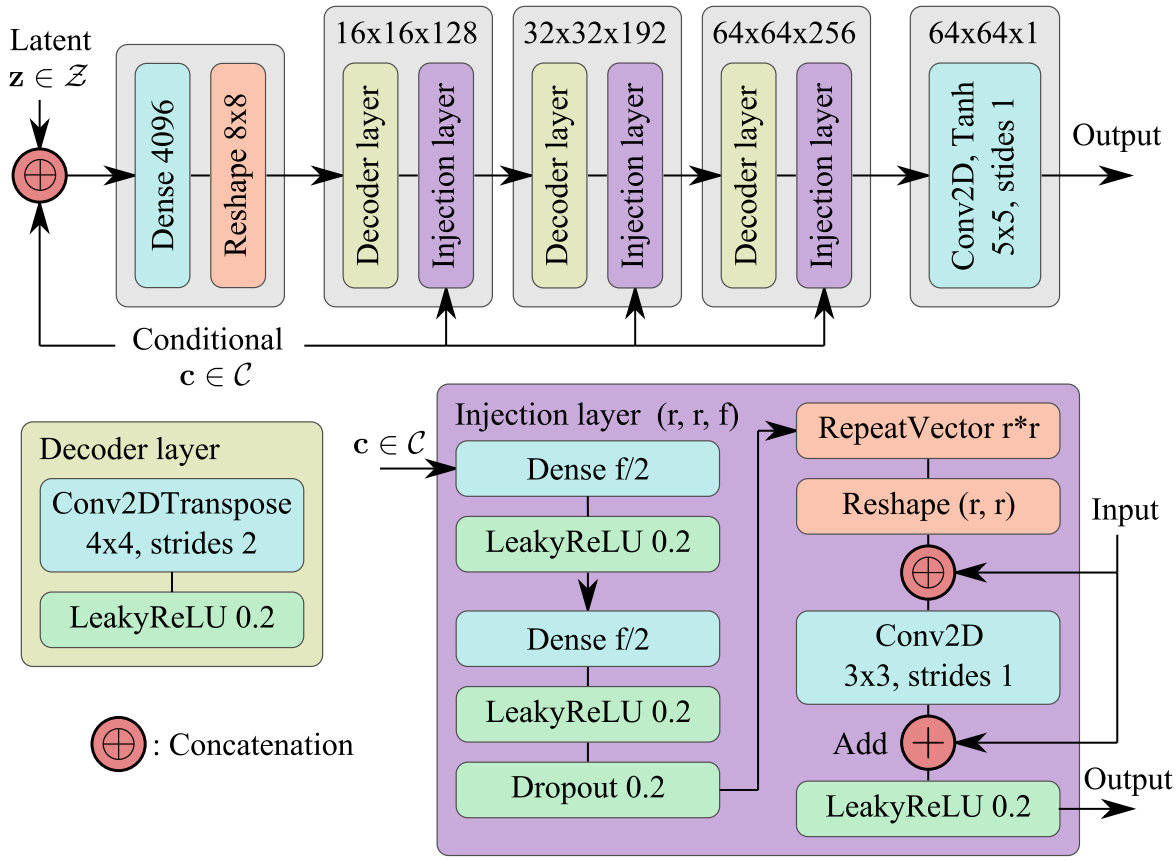

Figure 4.2.: SpinGAN (with purple injection layers) / DCGAN (without injection) generator. Numbers in the top of the gray boxes correspond to the resolution and filter/channel size of the layer. The parameters are given for the system size $L = 64$. Inputs are the latent vectors $\mathbf{z} \in \mathcal{Z}$ and condition $\mathbf{c} = (T,T,T,T)$ with $T \in \mathbb{R}^+$. At every injection layer, the condition is also provided. RepeatVector means to take a vector and create identical copies.

For the training process, we use the Adam optimizer [12] with the same parameters for the generator and discriminator: $(\beta_1 = 0, \beta_2 = 0.9)$. The learning rate has an exponential decay with an initial value of $\lambda = 3 \times 10^{-4}$ and a decay rate of 0.9 per 20 epochs.

5. Numerical experiments

5.1. Metrics

Generative networks behave special during training. For normal classification networks, the performance generally increases and converges with a longer training time, not considering overfitting. GANs on the other hand are more complex in their performance evolution over the training epochs, as mentioned in the convergence discussion of subsection 1.4.2. Therefore, we need a way to tell at which training epoch the GAN performed best. Another point is the comparability with other research papers. For these reasons, we introduce two metrics to measure the GAN performance.

Percentage overlap: The percentage overlap POL of two normalized binned distributions p_1 and p_2 is defined as

$$\mathrm{POL}(p_1, p_2) := \sum_{i}^{\mathrm{bins}} \min \left[p_1^{(i)}, p_2^{(i)} \right]. \tag{5.1}$$

Here i is the bin index and $p_{1,2}^{(i)}$ the value of the i-th bin of the corresponding distribution. We use this metric to measure the similarity of observable histograms between the reference Monte Carlo and generated data. A higher overlap is better. The metric is insufficient in the sense that a high percentage overlap does not mean close mean observables.

Observable distance: For physical application, the generator should generate data that includes the correct observable averages. We define the observable distance as

$$\text{Observable distance} := \sqrt{\frac{1}{N} \sum_{i=1}^{N} \left(\frac{x_{\mathrm{GAN},i} - x_{\mathrm{MC},i}}{\sigma_{\mathrm{MC},i}} \right)^2}, \tag{5.2}$$

where x_i are the means of the considered observables at a given temperature T and σ_i is the corresponding standard deviation. Both are either from GAN or the reference Monte Carlo (MC) data. In our case, we utilize the observables $|m|, E, \chi, \xi$ from section 2.1 and additional variables U_2, κ_3 to account for higher moments. The latter are the Binder

cumulant U_2 [3] and third cumulant κ_3 of the magnetization, defined as:

$$U_2 := \frac{3}{2}\left(1 - \frac{\langle m^4 \rangle}{3\langle m^2 \rangle^2}\right) \tag{5.3}$$

$$\kappa_3 := \frac{N}{T}\left(\langle |m|^3 \rangle - 3\langle m^2 \rangle \langle |m| \rangle + 2\langle |m| \rangle^3\right) \tag{5.4}$$

With the observable distance, we can judge the physical performance of our proposed methods. Especially, the best epoch within a training run can be identified as the one with the lowest observable distance.

5.2. Gan fidelity

A conditional GAN is able to generate states at any given temperature very quickly and efficiently. This allows us to differentiate actual states, in the sense of latent vectors/states $\mathbf{z}$, depending on thermodynamic control parameters. We expect the change of state to peak in the vicinity of a phase transition. This would yield a new way to detect phase transitions in unknown systems. Hence, we define the GAN fidelity $\mathcal{F}_{\text{GAN}}$ as

$$\mathcal{F}_{\text{GAN}}(T) := \mathbb{E}_{\mathbf{z}\sim p}\left[\left|\frac{\partial G(\mathbf{z}, T)}{\partial T}\right|\right]. \tag{5.5}$$

Here the exact derivation is performed and does not need to be approximated. Neural-network frameworks are extremely optimized for calculating exact gradients (autograd). Therefore, we can take directly the derivative of the generated states with respect to the temperature T. For this we generate states, take the element-wise partial derivative and apply the absolute value. Then we average over elements of the latent space distribution. With this, we receive a new measure of the change of state depending on T.

5.3. Implementation details

The Monte Carlo simulation is implemented for performance reasons in C++. For the machine learning part, we used the Python interface of TensorFlow 2 [15]. The code is published in the repository:
`https://github.com/FlorianFuerrutter/gans-for-spin-models`.

All training runs are done on the GPU (RTX 3090) of a home PC. The training time was capped to 12 h maximum per training run. Due to memory constraints a maximum system size of $L = 64$ was considered.

Note that the training time limitation has to be considered while interpreting the results of this thesis. Modern architectures like StyleGAN2 [10] specify in their papers a training time of multiple days and utilize multiple GPU systems. Nevertheless, we show good results with our limited resources.

6. Model performance

We evaluate our conditional GANs by generating numerous samples at different temperatures and calculate the corresponding observables. For the observable calculation of MC and GAN data, we use Binning/Jackknife algorithms. The physical expectancy

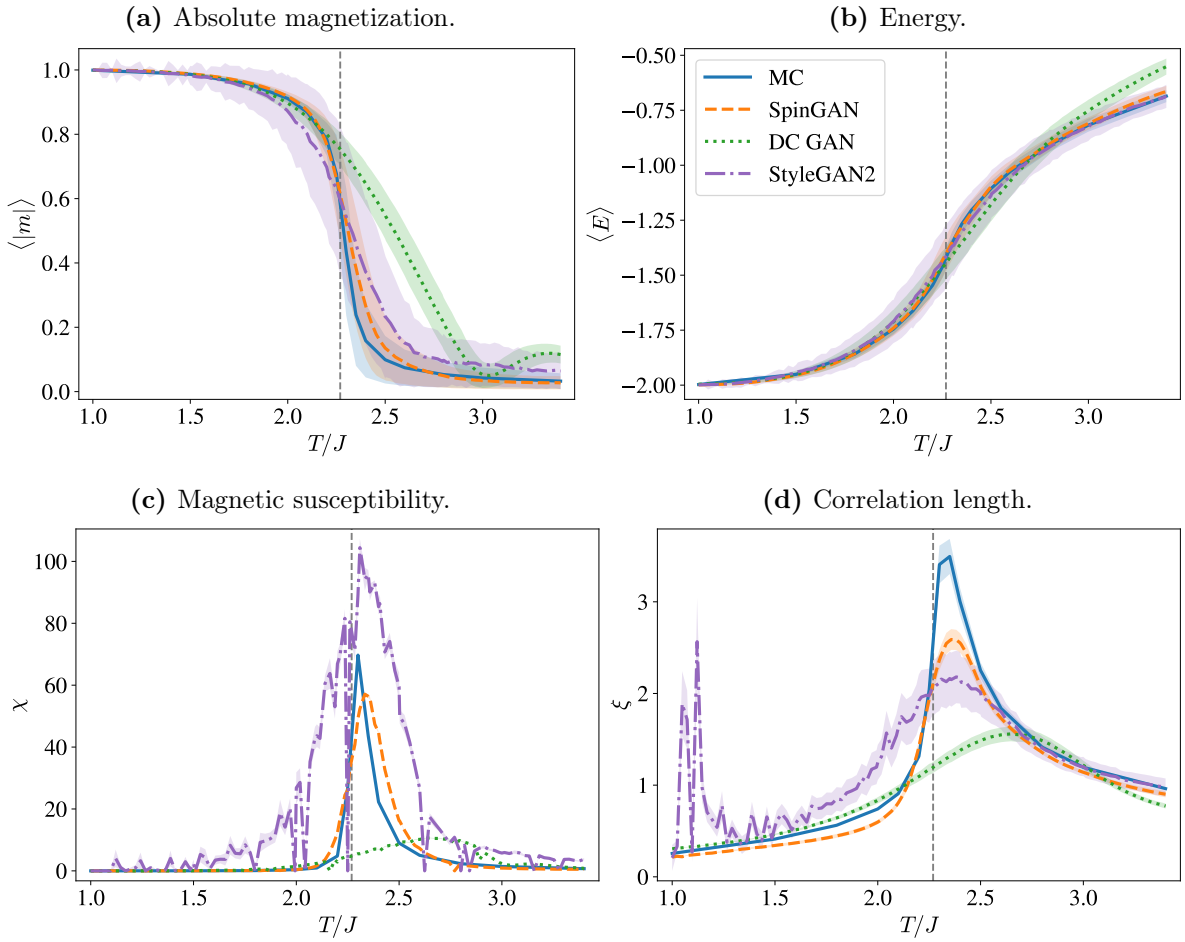

Figure 6.1.: Presented are the mean values of the observables for different GAN architectures. The shaded areas are the respective standard deviation. Monte Carlo (MC) data is used as the ground truth and a larger overlap corresponds to a better method. The critical temperature T_c is marked as a vertical line. The considered system size is $L = 64$. The MC data is from section 3.3 and the GAN is evaluated at 115 temperatures with 2^{14} samples each.

values of the observables should match the ones of the reference MC data. A higher overlap is better. We present a comparison of the GAN performances in Figure 6.1.

As we can see SpinGAN shows the best performance overall. The energy is almost perfect over the whole temperature range. In Figure 6.1a (magnetization) we see a deviation after the critical temperature. We call this behaviour overshoot and it is seen

Table 6.1.: Evaluation of the best mean observable distance of the considered GAN architectures. The observable distance is averaged over the 15 temperatures of the training set. A lower value is better and corresponds to closer values to the reference Monte Carlo data.

	$\mathbb{E}_T$ [observable distance]
DCGAN	95.4 ± 55.8
StyleGAN2	846.2 ± 1761.3
SpinGAN	32.6 ± 18.3

in all architectures. The magnetic susceptibility χ and correlation length ξ of SpinGAN shows distinct peaks without noise. Note, the overshoot of the χ peak. The correlation peak is at the correct position but not as high. We suspect that the generator misses out on the larger clusters in the MC data. To give a comparable metric we calculate the observable distance (Equation 5.2). The result is given in Table 6.1.

6.1. Overshoot and mode collapse

To analyze the overshoot of SpinGAN we look at the magnetization histograms at different temperatures, presented in Figure 6.2. We know the magnetization of the Ising model has a spontaneous symmetry breaking for $T < T_c$. Further, the MC data does not inherit the symmetry breaking because the mirrored states are considered of equal probability.

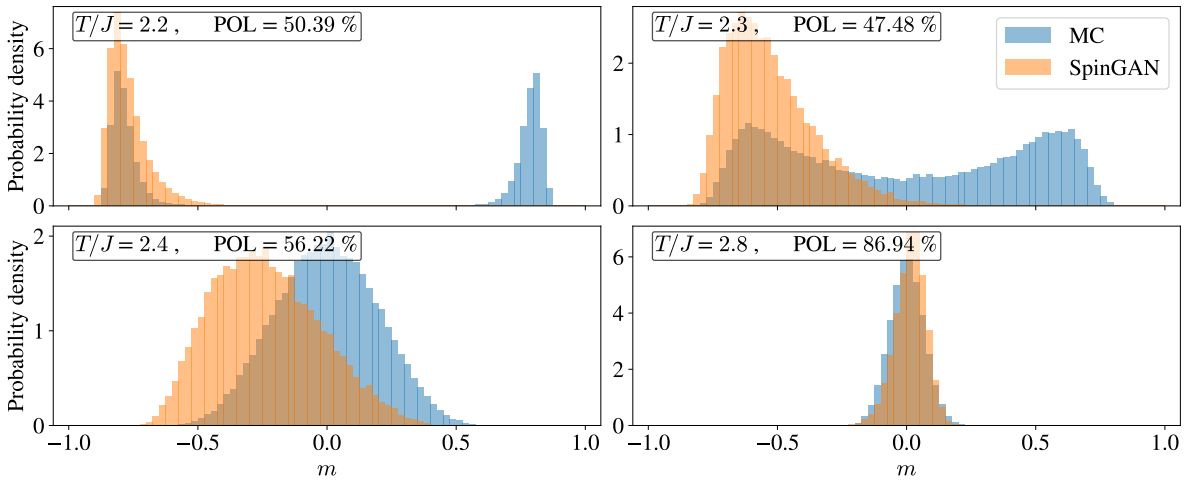

Figure 6.2.: Histograms of the magnetization for the system size $L = 64$ and different temperatures. Monte Carlo (MC) data is used as the ground truth and a larger overlap is better.

In Figure 6.2 we see that the GAN has a mode collapse (explained in subsection 1.4.2)

in one of the up or down directions and maps the actual symmetry breaking. In testing, it showed to improve the accuracy greatly if such a mode collapse occurred. Some model parameters led to no mode collapse with lower performance (e.g., Figure A.3b). The overshoot of the magnetization, seen in Figure 6.1a, can be explained with the shifted histograms. For $T < T_c$ the histograms have POL $\approx 50\,\%$ overlap with the MC data. Due to the symmetry, the relevant parameter $|m|$ has a POL $\approx 100\,\%$ matching. Over T_c

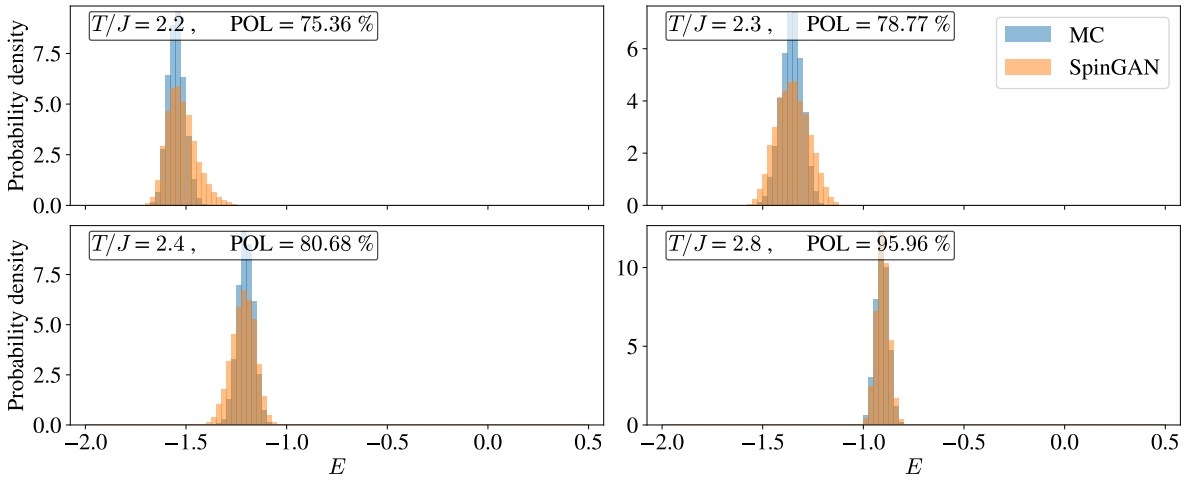

Figure 6.3.: Histograms of the energy for the system size $L = 64$ and different temperatures. Monte Carlo (MC) data is used as the ground truth and a larger overlap is better.

the histograms are shifted and catch up to an accurate percentage overlap with higher T. In Figure 6.3 the energy histograms are presented with an overall sufficient performance.

6.2. State evolution

The generator can be evaluated very efficiently and allows us to sample many states at an arbitrary temperature quickly. A remarkable property of our conditional generative model is that we are able to evolve single states (in the sense of latent vectors $\mathbf{z}$) completely deterministic through the temperature range. All we have to do is to fix a latent vector $\mathbf{z}$ and change the conditional input T. This is shown in Figure 6.4 and Figure A.1. We can follow a state and see how clusters emerge and the Ising model states change its phases. With classic Monte Carlo methods, an evolution of this kind is not possible. Randomness is introduced because of the stochastic property and MC simulations have to thermalize at every temperature step before evaluation.

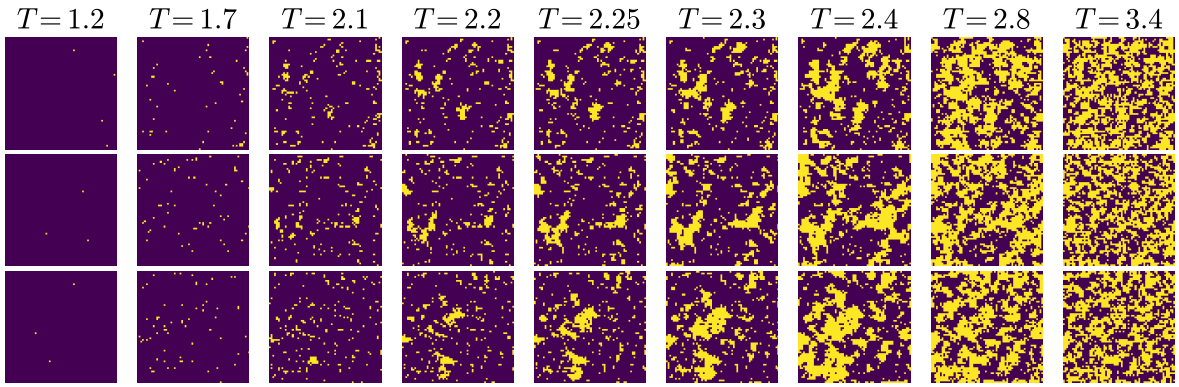

Figure 6.4.: States generated with SpinGAN, utilizing a system size of $L = 64$. The cols represent the same temperature T. For the rows three fixed latent vectors $\mathbf{z}$ are used. With the fixation in $\mathbf{z}$ and variation in T, a single state is evolved through the temperature range. On the left we see the ferromagnetic case with most spins aligned. Following a row to the right makes the emerging of clusters visible until thermodynamic fluctuations dominate and the paramagnetic phase takes over.

6.3. GAN fidelity

We evaluate Equation 5.5 for SpinGAN at different lattice sizes L (Figure 6.5). As discussed in section 5.2 we see peaks in the vicinity of the critical temperature. The peaks are not expected to be at T_c because fidelities of the finite system approach T_c from the right with larger L. Due to hyperparameter tuning, at each system size L, the latter is not seen strictly. Nevertheless, the curve of $L = 64$ shows a smooth peak.

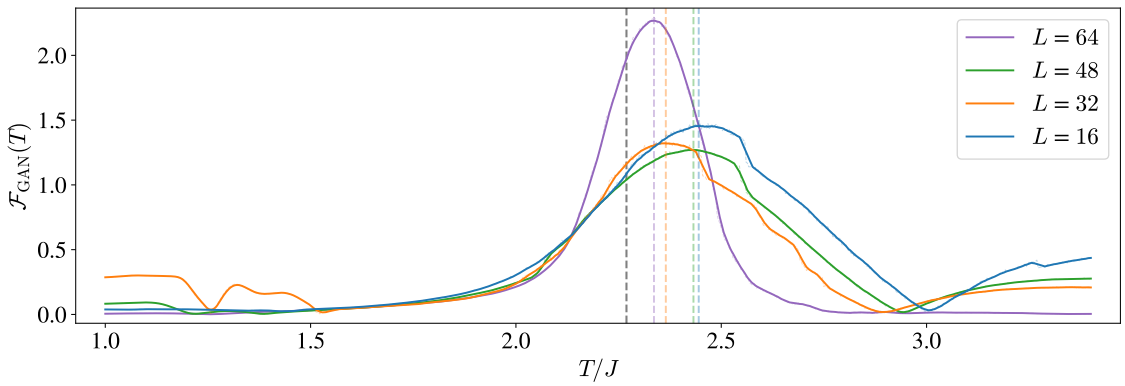

Figure 6.5.: The SpinGAN fidelity $\mathcal{F}_{\mathrm{GAN}}$ for different system sizes L. T_c is marked as a gray line. Coloured vertical lines represent the maximum of their corresponding curve.

With vanishing $\mathcal{F}_{\mathrm{GAN}}$ in the outer regions. This is because for $T < T_c$ the spins are aligned and do not change much. For $T > T_c$ the random fluctuations cancel each other in the average. Without knowledge of the system with its physical observables (e.g., ξ, χ) which normally indicate the phase transition, we proposed a method to directly calculate the change of the states depending on thermodynamic control parameters.

Summary, Conclusion and Outlook

We studied the machine learning technique of generative adversarial networks (GAN) and applied it to the famous Ising model. As a training set, we used Monte Carlo simulation to create Ising configuration at 15 distinct temperature points. The GAN generates states conditioned on the temperature T. This allowed us to generate configurations at unseen temperatures which were not included in the training set.

We proposed the SpinGAN architecture which is able to outperform the other utilized models. Furthermore, the resulting expectation values of the Ising model observables, compared to the reference Monte Carlo data, are remarkably accurate. The absolute magnetization differs only slightly in a small region after the critical temperature (overshoot). A mode collapse following the spontaneous symmetry breaking was observed which improved the accuracy greatly. SpinGANs capability to 'learn' the phase transition and the state dependency on the temperature allowed us to look further into the Ising state behaviour. We were able to evolve single distinct states through the temperature range. With this, we got insights into how spin clusters emerge. Last but not least, we evaluated the GAN fidelity exactly and presented the peak in the change of state in the vicinity of the critical temperature.

The results of this thesis could be improved with longer training times. Especially, the StyleGAN2 architecture showed an improvement after 10 h training and in the paper they mention a training time of a few days. Furthermore, GPU clusters would allow for larger networks to be trained, and an overall accuracy boost could be achieved.

Using the ideas of this thesis one could apply conditional GANs to the 3D Ising model or entirely different spin models. Because normally no analytical result is known the GAN technique could help us to gain a deeper understanding of the models. Further, the GAN fidelity could be used to identify critical temperatures of physical systems. Another possibility is to use other conditional parameters additional to the temperature (e.g., the external field of the Ising model h) and let the GAN learn the state dependency.

References

[1] M. Arjovsky and L. Bottou. "Towards Principled Methods for Training Generative Adversarial Networks". In: (Jan. 17, 2017). arXiv: 1701.04862 [stat.ML].

[2] M. Arjovsky, S. Chintala, and L. Bottou. "Wasserstein GAN". In: (Jan. 26, 2017). arXiv: 1701.07875 [stat.ML].

[3] K. Binder. "Critical Properties from Monte Carlo Coarse Graining and Renormalization". In: *Phys. Rev. Lett.* 47 (1981), pp. 693–696. DOI: 10.1103/PhysRevLett.47.693.

[4] K. Fukushima. "Neocognition: A self-organizing neural network model for a mechanism of pattern recognition unaffected by shift in position". English. In: *Biological Cybernetics* 36 (1980), pp. 193–202. ISSN: 0340-1200. DOI: 10.1007/BF00344251.

[5] I. J. Goodfellow et al. "Generative Adversarial Networks". In: (June 10, 2014). arXiv: 1406.2661 [stat.ML].

[6] W. K. Hastings. "Monte Carlo Sampling Methods Using Markov Chains and Their Applications". In: *Biometrika* 57 (1970), pp. 97–109. DOI: 10.1093/biomet/57.1.97.

[7] K. Hornik, M. Stinchcombe, and H. White. "Multilayer feedforward networks are universal approximators". In: 2 (1989), pp. 359–366. ISSN: 0893-6080. DOI: 10.1016/0893-6080(89)90020-8.

[8] E. Ising. "A contribution to the theory of ferromagnetism". German. In: *Zeitschrift für Physik* 31 (1925), pp. 253–257. ISSN: 0939-7922. DOI: 10.1007/BF02980577.

[9] T. Karras, S. Laine, and T. Aila. "A Style-Based Generator Architecture for Generative Adversarial Networks". In: (Dec. 12, 2018). arXiv: 1812.04948 [cs.NE].

[10] T. Karras et al. "Analyzing and Improving the Image Quality of StyleGAN". In: *CoRR* abs/1912.04958 (2019). arXiv: 1912.04958. URL: http://arxiv.org/abs/1912.04958.

[11] H. G. Katzgraber. "Introduction to Monte Carlo Methods". In: (May 11, 2009). arXiv: 0905.1629 [cond-mat.stat-mech].

[12] D. P. Kingma and J. Ba. "Adam: A Method for Stochastic Optimization". In: *arXiv e-prints*, arXiv:1412.6980 (Dec. 2014). arXiv: 1412.6980 [cs.LG]. URL: https://ui.adsabs.harvard.edu/abs/2014arXiv1412.6980K.

[13] Y. Lecun et al. "Gradient-based learning applied to document recognition". In: *Proceedings of the IEEE* 86 (11 1998), pp. 2278–2324. ISSN: 1558-2256. DOI: 10.1109/5.726791.

[14] Z. Liu, S. P. Rodrigues, and W. Cai. "Simulating the Ising Model with a Deep Convolutional Generative Adversarial Network". In: (Oct. 13, 2017). arXiv: 1710.04987 [cond-mat.dis-nn].

[15] Martín Abadi et al. *TensorFlow: Large-Scale Machine Learning on Heterogeneous Systems*. Software available from tensorflow.org. 2015. URL: https://www.tensorflow.org/.

[16] W. S. McCulloch and W. Pitts. "A logical calculus of the ideas immanent in nervous activity". In: 5 (1943), pp. 115–133. ISSN: 0007-4985. DOI: 10.1007/bf02478259.

[17] L. Mescheder, A. Geiger, and S. Nowozin. "Which Training Methods for GANs do actually Converge?" In: *International Conference on Machine Learning 2018* (Jan. 13, 2018). arXiv: 1801.04406 [cs.LG].

[18] K. Mills and I. Tamblyn. "Phase space sampling and operator confidence with generative adversarial networks". In: *arXiv e-prints*, arXiv:1710.08053 (Oct. 2017). arXiv: 1710.08053 [cond-mat.stat-mech]. URL: https://ui.adsabs.harvard.edu/abs/2017arXiv171008053M.

[19] A. Odena, C. Olah, and J. Shlens. "Conditional Image Synthesis With Auxiliary Classifier GANs". In: (Oct. 30, 2016). arXiv: 1610.09585 [stat.ML].

[20] L. Onsager. "Crystal statistics. 1. A Two-dimensional model with an order disorder transition". In: *Phys. Rev.* 65 (1944), pp. 117–149. DOI: 10.1103/PhysRev.65.117.

[21] J. Qiang. "Monte Carlo Simulation Techniques". In: (June 18, 2020). arXiv: 2006.10506 [physics.comp-ph].

[22] A. Radford, L. Metz, and S. Chintala. "Unsupervised Representation Learning with Deep Convolutional Generative Adversarial Networks". In: (Nov. 19, 2015). arXiv: 1511.06434 [cs.LG].

[23] J. Singh et al. "Generative models for sampling and phase transition indication in spin systems". In: *SciPost Phys. 11, 043 (2021)* (June 21, 2020). DOI: 10.21468/SciPostPhys.11.2.043. arXiv: 2006.11868 [cond-mat.stat-mech].

[24] J.-C. Walter and G. Barkema. "An introduction to Monte Carlo methods". In: (Apr. 1, 2014). DOI: 10.1016/j.physa.2014.06.014. arXiv: 1404.0209 [cond-mat.stat-mech].

[25] P. Werbos. "Beyond Regression: New Tools for Prediction and Analysis in the Behavioral Science. Thesis (Ph. D.)." PhD thesis. Appl. Math. Harvard University, Jan. 1974.

[26] U. Wolff. "Collective Monte Carlo Updating for Spin Systems". In: *Phys. Rev. Lett.* 62 (4 Jan. 1989), pp. 361–364. DOI: 10.1103/PhysRevLett.62.361. URL: https://link.aps.org/doi/10.1103/PhysRevLett.62.361.

[27] A. Yu et al. "Arbitrary-Depth Universal Approximation Theorems for Operator Neural Networks". In: (Sept. 23, 2021). arXiv: 2109.11354 [cs.LG].

A. Additional performance data

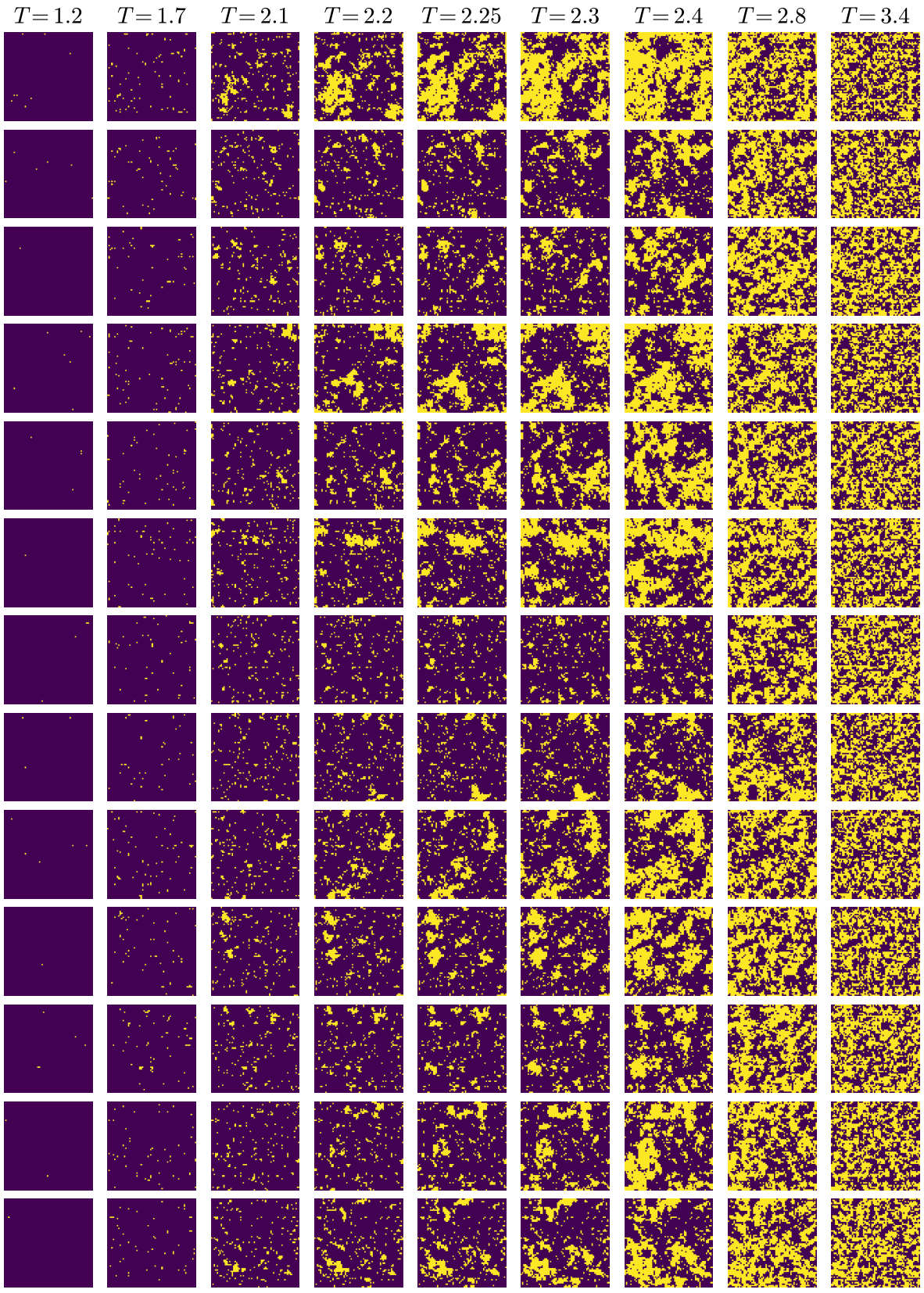

Figure A.1.: States generated with SpinGAN, utilizing a system size of $L = 64$. The cols represent the same temperature T. For the rows fixed latent vectors $\mathbf{z}$ are used. With the fixation in $\mathbf{z}$ and variation in T, a single state is evolved through the temperature range.

A.1. SpinGAN

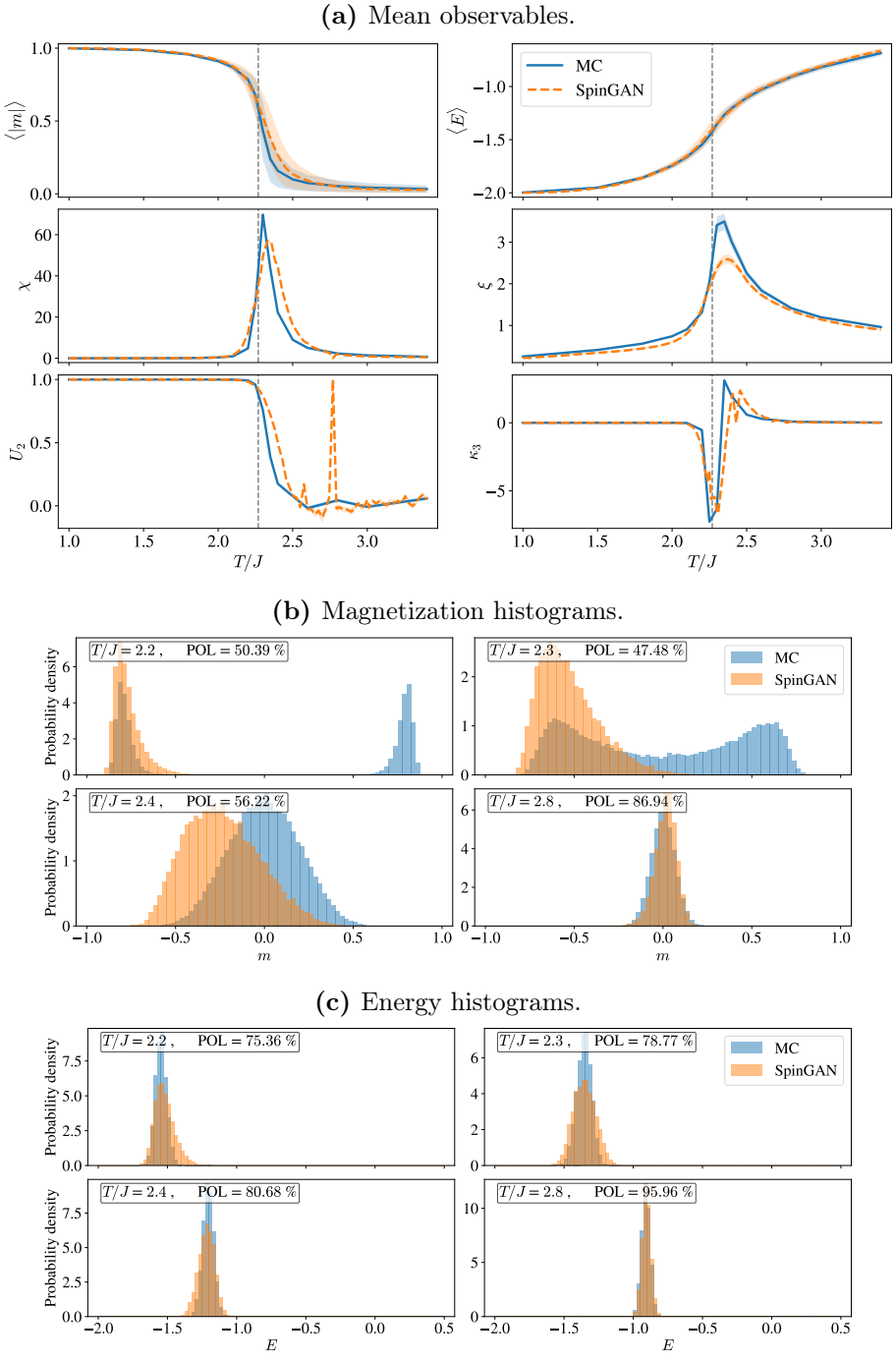

Figure A.2.: SpinGAN; (a) mean values of the observables, where shaded areas are the respective standard deviation. Histograms of the magnetization (b) and energy (c). In (a) the critical temperature T_c is marked as a vertical line. Monte Carlo (MC) data is used as the ground truth, a larger overlap is better. The used system size is $L = 64$.

A.2. StyleGAN2

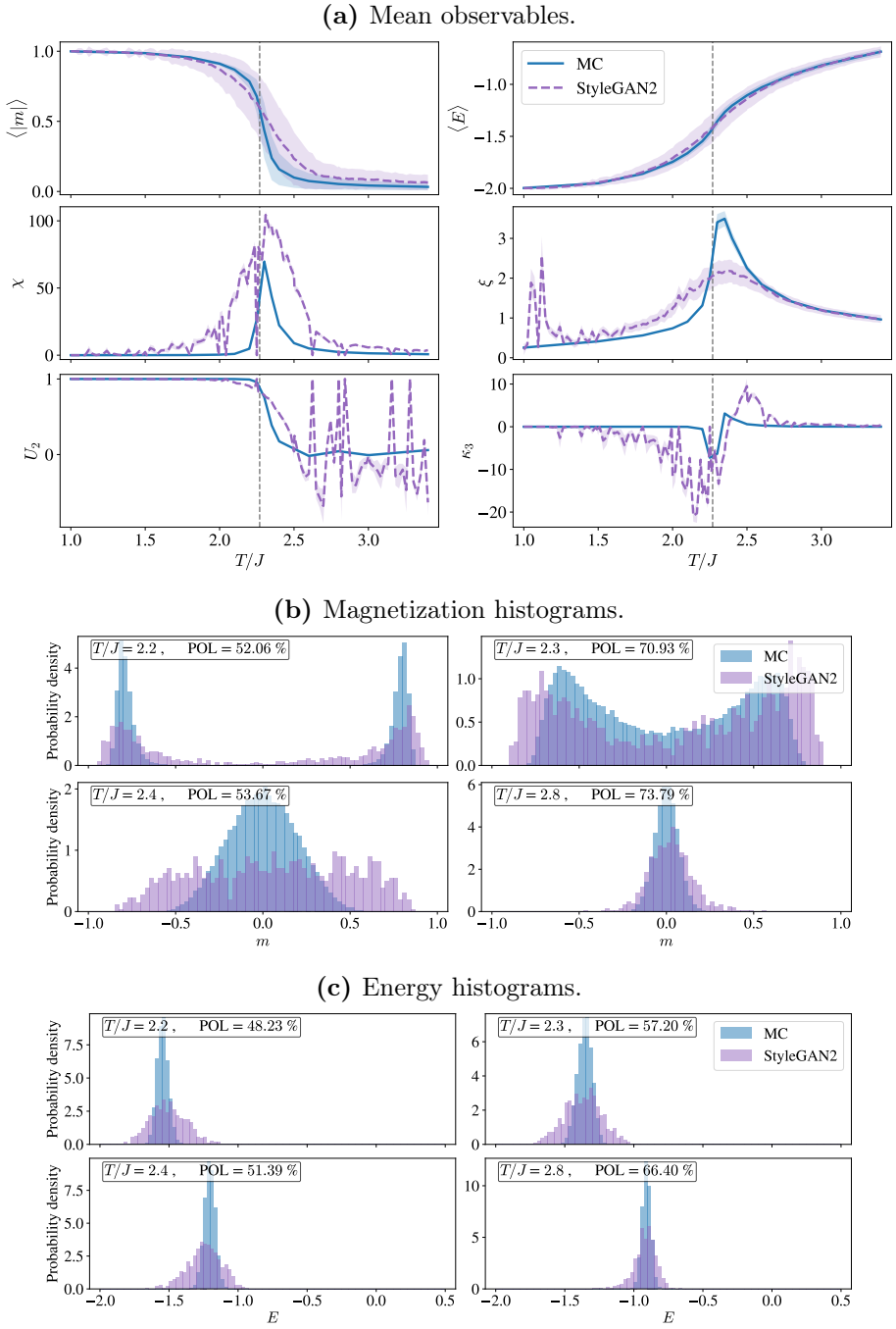

Figure A.3.: StyleGAN2; (a) mean values of the observables, where shaded areas are the respective standard deviation. Histograms of the magnetization (b) and energy (c). In (a) the critical temperature T_c is marked as a vertical line. Monte Carlo (MC) data is used as the ground truth, a larger overlap is better. The used system size is $L = 64$.

A.3. DCGAN

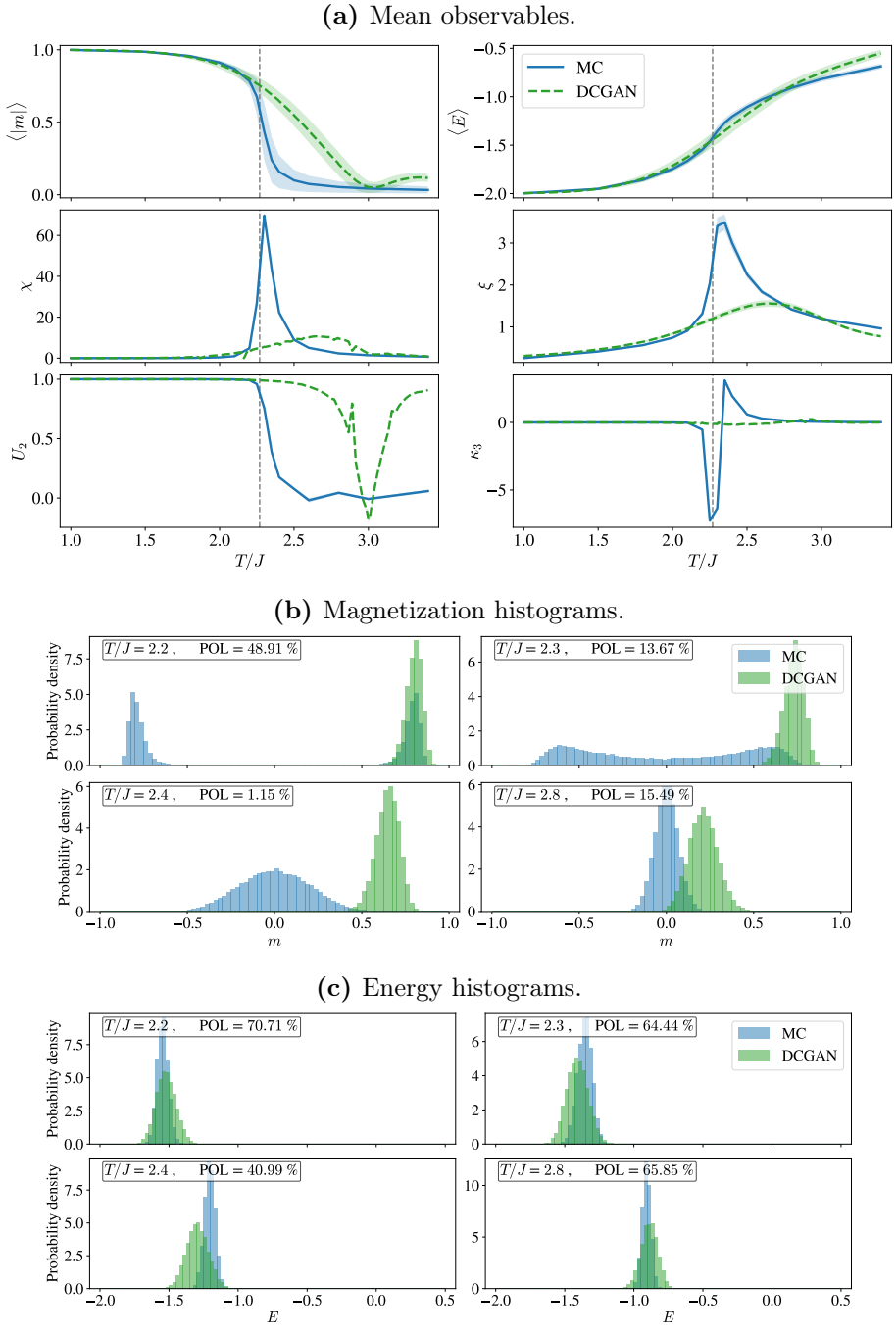

Figure A.4.: DCGAN; (a) mean values of the observables, where shaded areas are the respective standard deviation. Histograms of the magnetization (b) and energy (c). In (a) the critical temperature T_c is marked as a vertical line. Monte Carlo (MC) data is used as the ground truth, a larger overlap is better. The used system size is $L = 64$.

B. Theorem proofs

The proofs of the theorems mentioned in the section 2.1 of the Ising model chapter.

Theorem B.0.1. *The magnetic susceptibility can be evaluated with fluctuations of the magnetization in thermodynamic equilibrium*

$$\chi = \left(\frac{\partial m}{\partial h}\right)_{T,\, h=0} = \frac{N}{k_B T} \operatorname{Var}\left[|m|\right] = \frac{N}{k_B T} \left(\left\langle m^2 \right\rangle - \left\langle |m| \right\rangle^2\right). \tag{B.1}$$

Proof. Either use the fluctuation-response theorem for $M = Nm$ or evaluate the derivative directly. Notating $Z = Z(T, h)$ the partition function and $\beta = 1/k_{\mathrm{B}}T$:

$$\begin{aligned}
\left(\frac{\partial m}{\partial h}\right)_{T,\, h=0} &= \left(\frac{\partial}{\partial h}\frac{1}{NZ}\operatorname{Tr}\left[M\exp(-\beta H)\right]\right)_{T,\, h=0} \\
&= \left(-\frac{1}{NZ^2}\operatorname{Tr}\left[M\exp(-\beta H)\right]\frac{\partial Z}{\partial h} + \frac{1}{NZ}\operatorname{Tr}\left[M\frac{\partial}{\partial h}\exp(-\beta H)\right]\right)_{T,\, h=0} \\
&= \left(-\frac{\beta}{NZ^2}\operatorname{Tr}\left[M\exp(-\beta H)\right]^2 + \frac{\beta}{NZ}\operatorname{Tr}\left[M^2\exp(-\beta H)\right]\right)_{T,\, h=0} \\
&= -N\beta\left\langle m\right\rangle^2 + N\beta\left\langle m^2\right\rangle \\
&= N\beta\left(\left\langle m^2\right\rangle - \left\langle |m|\right\rangle^2\right).
\end{aligned} \tag{B.2}$$

In the last step we used the substitution $m \mapsto |m|$. We are allowed to do so because it changes nothing. In the paramagnetic phase where $m = 0$ it is clear and in the ferromagnetic regime the sign of $m \neq 0$ is not relevant for the physical behaviour, the up or down orientation is arbitrary. The substitution reason is the Monte Carlo simulation, where states with the same energy have the same probability and therefore $\langle m \rangle$ would be always zero $\forall T$. In that sense the spontaneous symmetry breaking is missed out and we account for that with the absolute magnetization. □

Theorem B.0.2. *The spin-spin correlation function can be calculated efficiently with a fast Fourier transform:*

$$G_c(\mathbf{r}) = (\mathcal{F}^{-1} g_c)(\mathbf{r}) \quad \text{with} \quad g_c(\mathbf{k}) = \frac{1}{N} \begin{cases} \left\langle |(\mathcal{F}\sigma_i)(\mathbf{k})|^2 \right\rangle : & \mathbf{k} \neq 0 \\ 0 : & \mathbf{k} = 0 \end{cases}. \tag{B.3}$$

Proof. With Equation 2.11 we could calculate G_c directly for all $\mathbf{r}$ with a time effort of $\mathcal{O}(N^2)$. We are able to improve this, with applying a discrete Fourier transform

$$\begin{aligned} g_c(\mathbf{k}) = (\mathcal{F}G_c)(\mathbf{k}) =& \sum_{\mathbf{r}} \exp\left(-\mathrm{i}\frac{2\pi}{L}\mathbf{r}\cdot\mathbf{k}\right) G_c(\mathbf{r}) \\ =& \sum_{\mathbf{r}} \exp\left(-\mathrm{i}\frac{2\pi}{L}\mathbf{r}\cdot\mathbf{k}\right) \frac{1}{N} \sum_{i,j=0}^{N-1} \delta_{(\mathbf{r}_i - \mathbf{r}_j),\mathbf{r}} \left[\langle\sigma_i\sigma_j\rangle - \langle m\rangle^2\right] \\ =& \frac{1}{N} \sum_{i,j=0}^{N-1} \exp\left(-\mathrm{i}\frac{2\pi}{L}\left[\mathbf{r}_i - \mathbf{r}_j\right]\cdot\mathbf{k}\right) \left[\langle\sigma_i\sigma_j\rangle - \langle m\rangle^2\right] \\ =& \frac{1}{N} \left\langle \sum_{i=0}^{N-1} \exp\left(-\mathrm{i}\frac{2\pi}{L}\mathbf{r}_i\cdot\mathbf{k}\right)\left[\sigma_i - \langle m\rangle\right] \cdot \sum_{j=0}^{N-1} \exp\left(\mathrm{i}\frac{2\pi}{L}\mathbf{r}_j\cdot\mathbf{k}\right)\left[\sigma_j - \langle m\rangle\right] \right\rangle \\ =& \frac{1}{N} \left\langle \left| \sum_{i=0}^{N-1} \exp\left(-\mathrm{i}\frac{2\pi}{L}\mathbf{r}_i\cdot\mathbf{k}\right)\left[\sigma_i - \langle m\rangle\right] \right|^2 \right\rangle \\ =& \frac{1}{N} \left\langle \left|(\mathcal{F}\left[\sigma_i - \langle m\rangle\right])(\mathbf{k})\right|^2 \right\rangle. \end{aligned} \tag{B.4}$$

Note, in the last line the Fourier transform is d-dimensional because the σ_i are arranged in a lattice with positions $\mathbf{r}_i$. In our case it will be a 2D transform over a microstate $\mathbf{\Sigma}$. A further simplification can be made with substituting $\sigma_i - \langle m\rangle \mapsto \sigma_i$. We get

$$g_c'(\mathbf{k}) = \frac{1}{N} \left\langle |(\mathcal{F}\sigma_i)(\mathbf{k})|^2 \right\rangle. \tag{B.5}$$

If we fix $g_c'(0) = 0$ then $g_c' = g_c$. This results from the definition of the Fourier transform where $\mathbf{k} = 0$ is just the average. In other words we remove the offset $\langle m\rangle$ afterwards.

In the implementation we calculate the fast Fourier transform (FFT) of σ_i for samples $\mathbf{\Sigma}$ and take the elements-wise absolute square. Then we evaluate Equation B.5 and set $g_c'(0) = 0$. The final result can then be inverse fast Fourier transformed. This yields directly $G_c(\mathbf{r})$ with a time effort of $\mathcal{O}(N \log N)$. □

C. Algorithms

Listing of the update algorithms explained in chapter 3 (Metropolis–Hastings and Wolff).

Algorithm C.1 Metropolis–Hastings algorithm, update

```
1:  function UpdateMetropolis(Σ, T, J)
2:      for x=0, N-1 do                                   ▷ N flip attempts
3:          i ← rndInteger[0, N − 1]                      ▷ Choose random spin
4:
5:          p^(i)_proposal ← ...                          ▷ Probability of flipping spin i
6:
7:          if (rndFloat[0, 1] ≤ p^(i)_proposal) then     ▷ Sample p^(i)_proposal
8:              σ_i ← (−σ_i)                              ▷ Flip spin i, update Σ
9:          end if
10:     end for
11: end function
```

Algorithm C.2 Wolff algorithm, update

```
1:  function UpdateWolff(Σ, T, J)
2:      p_append ← [1 − exp(−2β|J|)]                      ▷ Probability of extending the cluster
3:
4:      i ← rndInteger[0, N − 1]                          ▷ Choose random cluster starting spin
5:      σ_init ← σ_i                                      ▷ Store initial spin for alignment checks
6:      σ_i ← (−σ_i)                                      ▷ Flip starting spin
7:      cluster ← add spin i                              ▷ Add first spin to the cluster list
8:
9:      while cluster.size > 0 do
10:         k ← cluster.popBack                           ▷ Pop last entry in cluster list
11:
12:         for all neighbors of side k do
13:             if (σ_init == σ_neighbor) and (rndFloat[0, 1] ≤ p_append) then
14:                 cluster ← add neighbor spin           ▷ Extend the cluster
15:
16:                 σ_neighbor ← (−σ_neighbor)            ▷ Flipping spins on the fly
17:             end if
18:         end for
19:     end while
20: end function
```